2005

Magnetic Flux Sensor for Hearing and Application

Crystal R. Kenney

MAGNETIC FLUX SENSOR FOR HEARING AID APPLICATION

By

Crystal R. Kenney

B.S. University of Maine, 2003

A THESIS

Submitted in Partial Fulfillment of the

Requirements for the Degree of

Master of Science

(in Electrical Engineering)

The Graduate School

The University of Maine

August, 2005

Advisory Committee:

David E. Kotecki, Associate Professor of Electrical and Computer Engineering, Advisor

John Vetelino, Professor of Electrical and Computer Engineering

Donald Hummels, Professor of Electrical and Computer Engineering

MAGNETIC FLUX SENSOR FOR HEARING AID APPLICATION

By Crystal R. Kenney

Thesis Advisor: Dr. David E. Kotecki

An Abstract of the Thesis Presented
in Partial Fulfillment of the Requirements for the
Degree of Master of Science
(in Electrical Engineering)
August, 2005

A 3-D microelectronic inductor has been fabricated and characterized for use as a magnetic flux sensor, also known as a telecoil, for a hearing aid application. This telecoil was fabricated in a 0.5μm CMOS process with three metal layers. The 3-D structure is more space efficient than conventional spiral inductors and allows for an optimal number of turns for the space available. The telecoil has an inductance of 80μH, a resistance of 34kΩ, and a capacitance of 275pF.

The integrated telecoil acts as a magnetic flux sensor by picking up the magnetic signal from the phone speaker. The integrated telecoil is smaller than commercially available telecoils, which may allow telecoils to be available in all types of hearing aids. The electrical response of the telecoil to a changing magnetic field is linear with respect to the input amplitude. Neglecting the noise associated with lower frequencies, it is shown that the telecoil response is not dependent on frequency, which agrees with theory. The magnitude of the telecoil signal is of the form of $A + \frac{B}{r^3}$ where r is the distance between the speaker and telecoil, which differs from the theory. The increase in response due to the addition of a permeable core is much lower than expected.

When the telecoil is combined with a high-gain low-noise amplifier, it can easily be integrated with existing microelectronic hearing aid designs. Therefore the Cherry

Hooper amplifier and a single-ended amplifier were investigated. A single stage Cherry Hooper amplifier design was simulated at a gain of 29 dB, THD of -50dB, and equivalent input noise of $2.01\frac{nV}{\sqrt{Hz}}$. A three stage Cherry Hooper design (identical stages) with a filter has a simulated gain of 84 dB, THD of -49dB, and equivalent input noise of $2.01\frac{nV}{\sqrt{Hz}}$. The three stage amplifier also has a bandwidth of 3kHz and a driving capacity of 30pF external load capacitance. The complete single-ended amplifier design was simulated at a gain of 67dB, THD of -48dB, equivalent input noise of $45.3\frac{nV}{\sqrt{Hz}}$, and driving capacity of 1nF external load capacitance. More research is needed to obtain conclusive experimental parameters of the amplifiers.

ACKNOWLEDGMENTS

The student involved in this work was supported by a fellowship from the National Science Foundation (NSF) GK-12 Sensors! program under grant number NSF0139324. The original idea for this research was conceptualized by Richard Thibodeau, formally of Tibbits Industries.

Thanks to my family and friends for being supportive and understanding. A special thanks to my husband, James, for keeping me focused and sane. Thanks to Professor Kotecki for being my advisor and mentor for part of my undergraduate and throughout my graduate research at UMaine. Thanks to Professor Hummels for all of the help with MATLAB and LaTeX. Thanks to Professor Vetelino for the opportunities involved with the NSF-GK12 Sensors! program. Thanks to Al Whitney for being an excellent educator and always being there to help when I needed it.

TABLE OF CONTENTS

ACKNOWLEDGMENTS ii

LIST OF TABLES v

LIST OF FIGURES vi

Chapter

1 INTRODUCTION 1
- 1.1 Background 1
- 1.2 Purpose of the Research 3
- 1.3 Thesis Organization 5

2 TELECOIL PHYSICS 6
- 2.1 Faraday's Law of Induction 6
- 2.2 Lossy Modifications to Faraday's Law 10

3 TELECOIL DESIGN AND TESTING 13
- 3.1 Telecoil Layout 13
- 3.2 Testing 18
- 3.3 Summary 25

4 AMPLIFIER DESIGN 28
- 4.1 Cherry Hooper Design 28
  - 4.1.1 Circuit Design 28
  - 4.1.2 Circuit Performance 29
  - 4.1.3 Physical Design 35
  - 4.1.4 Experimental Results 37
- 4.2 Single Ended Amplifier 37
  - 4.2.1 Circuit Design 37
  - 4.2.2 Circuit Performance 39
  - 4.2.3 Physical Design 43
  - 4.2.4 Experimental Results 46

5 CONCLUSIONS AND FUTURE WORK 48

REFERENCES 51

APPENDIX A. Directions for Setup of Agilent 35670A Spectral Analyzer 53

APPENDIX B. Labview Subproject 55

LIST OF FIGURES

Figure 1.1 System level block diagram showing a complete hearing aid signal processing system..... 2

Figure 1.2 Example size of several telecoils..... 4

Figure 2.1 Signal reception from a telephone speaker..... 7

Figure 2.2 Component representation of function generator, speaker, and telecoil..... 11

Figure 3.1 Final Chip 14

Figure 3.2 Picture of the fabricated fuse..... 18

Figure 3.3 Testing apparatus configuration..... 19

Figure 3.4 Signal from changing magnetic flux..... 20

Figure 3.5 Input response of telecoil versus frequency..... 20

Figure 3.6 Telecoil response vs input amplitude at 1kHz. 21

Figure 3.7 Speaker impedance as a function of frequency..... 22

Figure 3.8 emf_k as a function of frequency with V_S of 5V. 22

Figure 3.9 Graph of $\frac{emf_t}{emf_k}$ versus frequency..... 24

Figure 3.10 $\frac{emf_t}{emf_k}$ of telecoil with worn probe pads. 24

Figure 3.11 Reproducibility of $\frac{emf_t}{emf_k}$ versus frequency over time (no core). 25

Figure 3.12 Received signal amplitude vs distance of speaker..... 26

Figure 3.13 Example size of several commercial telecoils (left) and the integrated telecoil (right). 26

Figure 4.1 Cherry Hooper amplifier schematic..... 30

Figure 4.2 Single stage Cherry Hooper gain response. 30

Figure 4.3 Single stage Cherry Hooper THD response..... 31

Figure 4.4 Three stage Cherry Hooper with filter biasing..... 32

Figure 4.5 Three stage Cherry Hooper with filter THD response..... 32

Figure 4.6 Three stage Cherry Hooper with filter gain response..... 33

Figure 4.7 Three stage Cherry Hooper amplifier with filter AC response..... 34

Figure 4.8 Decoupling capacitance between stages. 34
Figure 4.9 Capacitance drive capability of three stage Cherry Hooper amplifier with filter. 35
Figure 4.10 Cherry Hooper amplifier layout. 36
Figure 4.11 Circuit diagram of preamplifier. 38
Figure 4.12 Circuit diagram of second stage of amplifier. 39
Figure 4.13 Circuit diagram of complete single-ended amplifier. 40
Figure 4.14 Simulation setup for single-ended amplifier and preamplifier. 41
Figure 4.15 Gain response of complete single-ended amplifier 42
Figure 4.16 THD of complete single-ended amplifier. 42
Figure 4.17 Single-ended amplifier with load capacitance. 43
Figure 4.18 Layout of preamplifier 44
Figure 4.19 Layout of second stage of single-ended amplifier. 44
Figure 4.20 Layout of complete single-ended amplifier. 45
Figure 4.21 Layout of complete design. 45
Figure 4.22 Preliminary result showing the output from integrated telecoil and amplifier. 46

Figure B.1 Front Panel 56
Figure B.2 GP-IB Setup 56
Figure B.3 Query X axis data. 57
Figure B.4 Manipulate X axis data. 57
Figure B.5 Query Y axis data. 57
Figure B.6 Manipulate Y axis data. 58

Figure C.1 Cherry Hooper Bonding Diagram 60
Figure C.2 Single Ended Bonding Diagram 62

CHAPTER 1

INTRODUCTION

1.1 Background

Hearing aids often make use of a magnetic flux sensor called a telecoil. A telecoil responds to magnetic flux variations rather than acoustic vibrations. There are two primary applications for telecoil compatible hearing aids. The first application is in conjunction with a conventional telephone. The sound from the telephone speaker is produced by an electromagnet operating on a diaphragm. In a hearing aid without a telecoil, a small microphone in the hearing aid picks up the acoustic signal from the diaphragm of the phone speaker and transfers it into an electric signal. The electric signal is then amplified and used to drive a speaker in the hearing aid. In contrast, the telecoil converts the magnetic signal from the electromagnet to an electric signal. The electric signal from the telecoil can then be fed into the same amplification sequence as the signal from the microphone as shown in Figure 1.1. The telecoil makes use of inductive coupling as opposed to acoustic coupling and produces a tone clear of acoustic interference.

The second application of a telecoil compatible hearing aid is called an Inductive Loop (IL) System. A portable IL System can simply consist of several loops of wire attached to an amplifier which plugs into the "line out" port on electrical equipment. More permanent installations require higher quality equipment to prevent "spillage" of sound outside the loop as well as added costs to hide evidence of the IL System from consumer view. Also, it has been shown that since using an IL system requires very little work or equipment to implement it is more cost efficient than a competitive FM system and therefore provides greater benefit to the consumer[2]. The basic principle

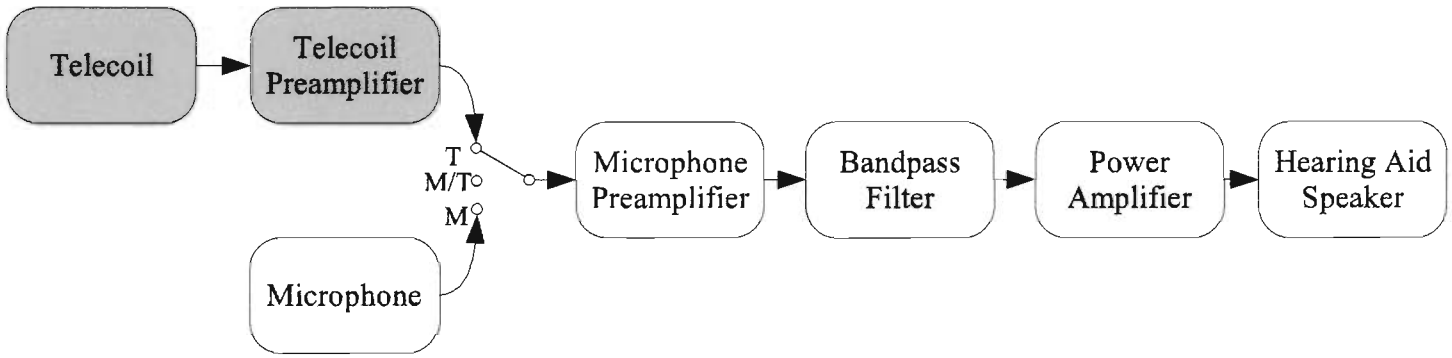

Figure 1.1: System level block diagram showing a complete hearing aid signal processing system[1]. The shaded grey blocks form the section addressed by this thesis.

underlying an IL System is that the telecoil inductively couples with the wire coil of the IL system instead of the electromagnet in a phone receiver.

Current hearing aids have several ways to access the signal from the telecoil. The most basic design uses a switch with a telecoil position (T) and a default microphone position (M). An M/T position (both microphone and telecoil active) has recently become popular. The M/T option primarily benefits students who participate in group projects and therefore need to hear their classmates as well as the teacher. Some hearing aids even offer a "touchless" T position so that when exposed to a strong magnetic signal the telecoil will automatically turn on[3].

The telecoil circuit is ideal for phone use, concert halls or anywhere a loudspeaker or public address (PA) system is used. In Europe (esp United Kingdom), concert halls have an IL System as a common service to their patrons. Concert halls in the US seem to rely on IR or FM communication systems which require bulky added equipment such as special microphones, speakers, and/or special headphones on each patron. Some of the IR or FM systems broadcast to a personal IL system around the neck, which then allows the telecoil in the patron's hearing aid to pick up the signal[2].

About 10% of the population would benefit from the use of hearing aides, and only 20% of those people who need them actually have hearing aides. Two common obstacles to getting a hearing aid are cost and vanity. People often do not want to admit they want a hearing aid or they do not want other people to know that they need one. Also, the hearing aid user almost always has to pay for a hearing aid themselves as very few health insurance policies cover hearing aid costs[4].

1.2 Purpose of the Research

Due to the miniaturization of telecoils (Figure 1.2), telecoils can now be included in almost all hearing aid models except the completely-in-the-canal (CIC) model (approximately 20% of the hearing aid market)[2]. However, commercial telecoils consist of

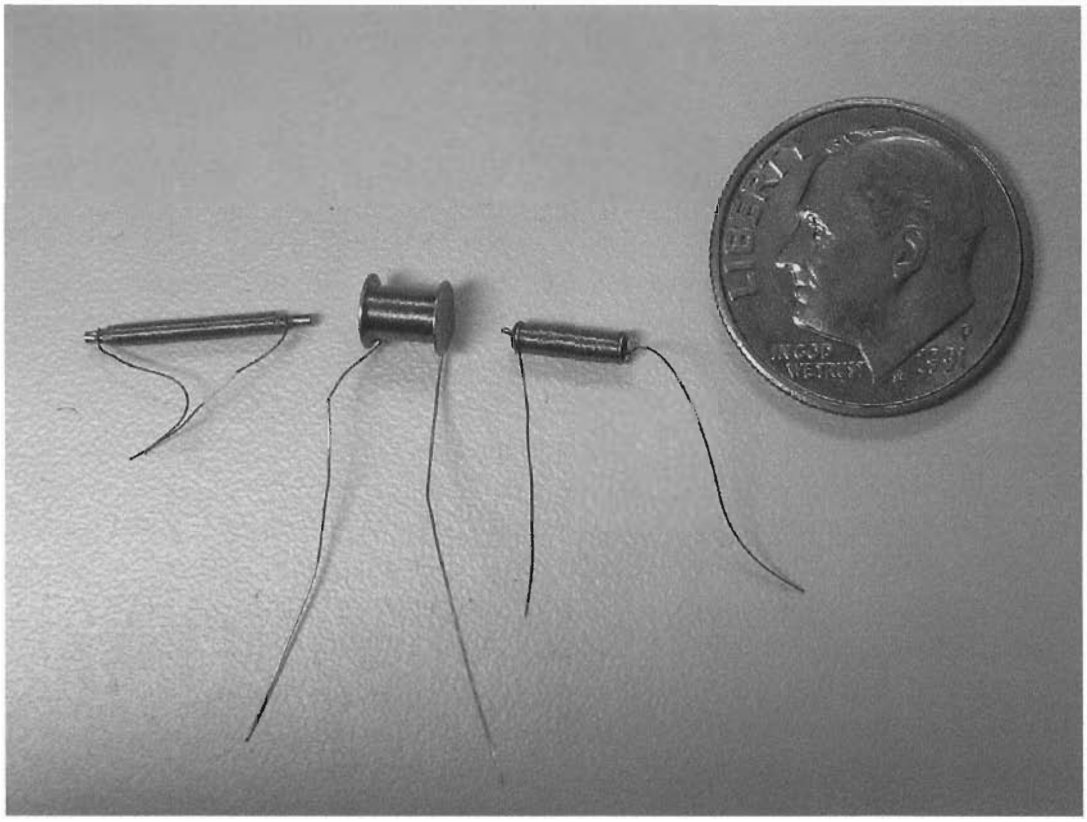

Figure 1.2: Example size of several telecoils.

thin wire wrapped around a permeable core by use of a mechanical winding machine[5]. This process produces low yield and high production costs which are passed onto the consumer. Therefore even though telecoils can be included in most hearing aids, not all hearing aid users want to bother with the added expense[3].

This research investigates a way to further reduce the size and cost of manufacturing telecoils by use of integrated semiconductor technology. Finding a way to implement a telecoil and a high-gain low-noise audio amplifier in an microelectronic technology would lower cost and size of telecoils. Therefore the prices of hearing aids could decrease and the hearing aid itself could become more discrete, encouraging more of the population to get their needed hearing aids.

This project concentrates on the integration of a telecoil and audio amplifier on a single integrated circuit. This combination could be combined with current hearing aid circuits to form a completely integrated hearing aid. A properly designed telecoil will maximize the number of turns of wire for the fabrication technology utilized as well as having a constant sheet resistance. The audio amplifier should be linear in the audio spectrum and have high gain and low noise.

1.3 Thesis Organization

This thesis is organized to give background information on the physics of telecoils, followed by the design and testing of telecoils, and then the design, simulation, and testing of low noise amplifier circuits combined with the telecoil.

Chapter 2 gives in depth information on the physics of telecoils.

Chapter 3 describes the design process and testing results of the telecoil.

Chapter 4 describes the design, implementation, and testing of two different analog amplifiers.

Chapter 5 gives a summery of the results as well as suggestions for future work.

CHAPTER 2

TELECOIL PHYSICS

2.1 Faraday's Law of Induction

A telecoil consists of many loops of wire surrounding a permeable core. According to Faraday's Law of Induction [6], the electric field induced in a closed loop is directly proportional to the rate of change of the magnetic flux through the surface bounded by that loop. This phenomenon is described by

$$\oint_C \vec{E} \cdot ds = -\frac{d\Phi_B}{dt} \tag{2.1}$$

where C is the closed loop, ds is a small section of the loop, $\vec{E}$ is the electric field and Φ_B is the magnetic flux. A telecoil has many turns of wire and therefore consists of many loops all connected together. The total induced voltage (emf) in the telecoil is therefore described by

$$emf = -N\frac{d\Phi_B}{dt} \tag{2.2}$$

where N is the number of wire loops in the telecoil.

Figure 2.1 shows a common hearing aid configuration[1] using a telecoil in conjunction with a telephone speaker. The signal from the telephone can send signals two different ways to the hearing aid. The first path involves the microphone. The diaphragm of the telephone speaker vibrates in the air and creates an acoustic signal. The microphone picks up the acoustic signal and translates it into an electronic signal. Signal processing is then employed with amplifiers and filters as shown in Figure 1.1. The second pathway takes the signal from the electromagnet in the telephone speaker. This electromagnet creates a changing magnetic field around the telephone speaker. When the consumer places their ear near the phone, a telecoil is able to measure this

$$emf = -N \frac{d\Phi_B}{dt}$$

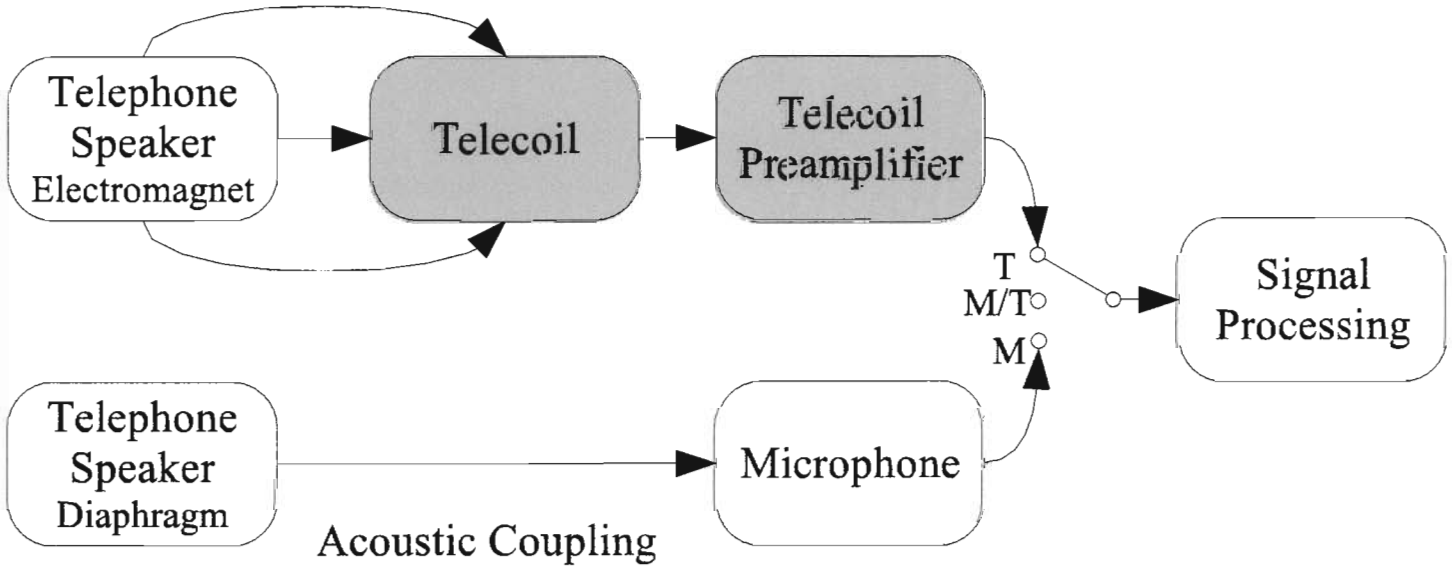

Figure 2.1: Signal reception from a telephone speaker. The shaded boxes represent the scope of this project.

signal as described by use of Faraday's Law of Induction (Equation 2.2). This signal is usually much smaller than the signal the microphone would pick up, so a preamplifier is required before reaching the rest of the hearing aid circuitry. The signal from the telecoil is void of acoustical interference.

Let the voltage across the inductance of the speaker emf_k be a sinusoidal voltage defined by

$$emf_k = K\sin(2\pi ft) \tag{2.3}$$

where K is the peak amplitude of the signal and f is the frequency of the signal. The speaker contains an electromagnet that follows Faraday's Law of Induction. Therefore, the magnetic flux Φ'_B 'created' by the electromagnet can be described by

$$\begin{aligned} \Phi'_B &= -\frac{1}{N_k}\int emf_k dt \\ &= \frac{1}{N_k 2\pi f} K\cos(2\pi ft) \end{aligned} \tag{2.4}$$

where N_k is the number of wire loops in the speaker.

The magnetic field strength H' induced depends on the geometry and material properties of the electromagnet as well as the magnetic flux. Therefore it can be described by

$$H' = \frac{M_k}{N_k 2\pi f} K\cos(2\pi ft) \tag{2.5}$$

where M_k is a constant defined by geometry, orientation and material properties.

The telecoil is located a distance r from the speaker. When the source of the magnetic field is a made up of loops as in an electromagnet and the distance r is much

larger than the radius of the loops, the magnetic field decreases as $\frac{1}{r^3}$[7]. Therefore the magnetic field H at the telecoil can be described by

$$H = \frac{mM_k}{N_k 2\pi f r^3} K \cos(2\pi f t) \tag{2.6}$$

where m is a constant of the intervening media.

The magnetic flux of the telecoil Φ_B also depends on geometry, orientation and material properties and is directly proportional to the area A encompassed by the loops. Therefore it can be described by

$$\Phi_B = \frac{mAM_k}{M_t N_k 2\pi f r^3} K \cos(2\pi f t) \tag{2.7}$$

where M_t is a constant defined by geometry, orientation and material properties.

The ideal voltage across the telecoil using Φ_B from Equation 2.7 and Equation 2.2 is described by

$$\begin{aligned} emf_t &= -N_t \frac{d\Phi_B}{dt} \\ &= \frac{N_t mAM_k}{M_t N_k r^3} K \sin(2\pi f t) \\ &= \frac{D}{r^3} \sin(2\pi f t) \end{aligned} \tag{2.8}$$

where

$$D = \frac{N_t mAM_k}{M_t N_k} K \tag{2.9}$$

Equation 2.8 shows that the magnitude of emf_t is independent of frequency assuming that the magnitude of emf_k, M_k, and M_t are independent of frequency. It also shows that emf_t decreases as $\frac{1}{r^3}$.

2.2 Lossy Modifications to Faraday's Law

The telephone speaker and the telecoil are not ideal. They both have significant resistance and the telecoil has significant capacitance. These non-ideal parameters cause both the speaker and the telecoil to be termed lossy. This means that a significant portion of the signal from V_S is lost before it contributes to the magnetic field strength. Figure 2.2 shows a model of the speaker and telecoil. It is assumed that the capacitance of the speaker is negligible at audio frequencies. The impedance of the speaker Z_K and the impedance of the telecoil Z_T are defined by

$$|Z_K| = \sqrt{R_K^2 + (2\pi f)^2 L_K^2} \tag{2.10}$$

$$|Z_T| = \left| \frac{R_T + sL_T}{1 + sR_T C_T + s^2 L_T C_T} \right| \tag{2.11}$$

where $s = j2\pi f$.

The physics presented thus far is valid assuming a couple clarifications. From Figure 2.2, the voltage that contributes to the creation of the magnetic field from the speaker emf_k can be described by

$$|emf_k| = \left| \frac{sL_K}{R_K + R_S + sL_K} \right| |V_S| \,. \tag{2.12}$$

The value of K in Equation 2.3 becomes a function of frequency given by

$$K = \left| \frac{sL_K}{R_K + R_S + sL_K} \right| K' \tag{2.13}$$

where V_S is sinusoidal with amplitude K' and K' is independent of frequency. Since the telecoil is not ideal, the signal picked up by the telecoil is attenuated over the length of the telecoil. The final voltage V_T will differ from the magnitude of emf_t by the amount described by

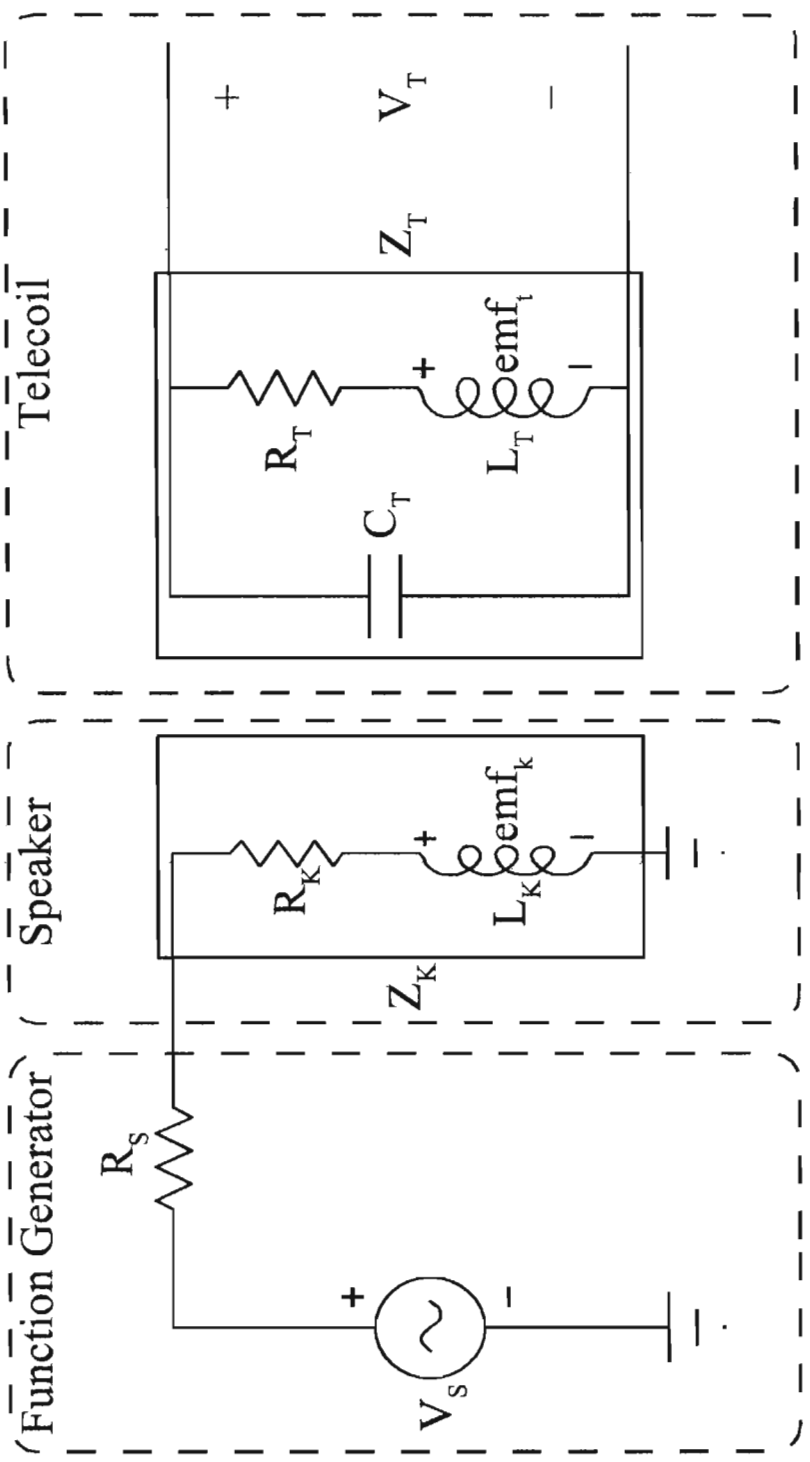

Figure 2.2: Component representation of function generator, speaker, and telecoil.

$$V_T = emf_t \left| \frac{\frac{1}{sC_T}}{R_T + \frac{1}{sC_T}} \right|$$
$$= emf_t \left| \frac{1}{1 + sR_T C_T} \right|. \quad (2.14)$$

Since the magnitude of emf_k is no longer independent of frequency, the resulting magnitude of emf_t and therefore the magnitude of V_T will also be dependent on frequency. However, the ratio of magnitudes of $\frac{emf_t}{emf_k}$ should be independent of frequency since the frequency component in both equations is confined to the parameter K. Also, emf_t and V_T will still be proportional to $\frac{1}{r^3}$ as described at the end of Section 2.1.

CHAPTER 3

TELECOIL DESIGN AND TESTING

3.1 Telecoil Layout

In a commercially available telecoil, the wire is wound around the permeable core, so that looking from the top, the wires are vertically stacked atop one another. In silicon design technology, there are a limited number of metal lines that can be stacked atop one another. In the AMI 0.5μm CMOS process, there are only three metal layers. In commercially available telecoils there are hundreds to thousands of metal loops around the core. Since the number of loops is directly proportional to magnetic response of the telecoil (Equation 2.2), the maximum possible number of turns is desired.

The integrated telecoil developed in this project uses all three possible metal layers. The bottom two metal layers are shorted together which produce a sheet resistance equal to the top metal layer. The telecoil consists of many small loops that alternate between metal layers as the telecoil winds further out. This allows the loops to be stacked on one another as much as possible and allows the maximum amount of turns[8]. The middle of the telecoil is left empty as an area to place a permeable core. Figure 3.1(a) shows the final layout and Figure 3.1(b) shows a picture of the fabricated chip.

There are two sets of chips fabricated as part of this project, but the telecoils used in both are identical. Therefore, the following information taken from phase one of the project should also be accurate for phase two. The total simulated resistance of the telecoil (R_L) is 34kΩ.

An estimate was made for the inductance of the telecoil by modifying equations used for a one layer spiral inductor[9]. The modified equations are given by Equation 3.1 through Equation 3.7, and the parameters used are shown in Table 3.1. The number of

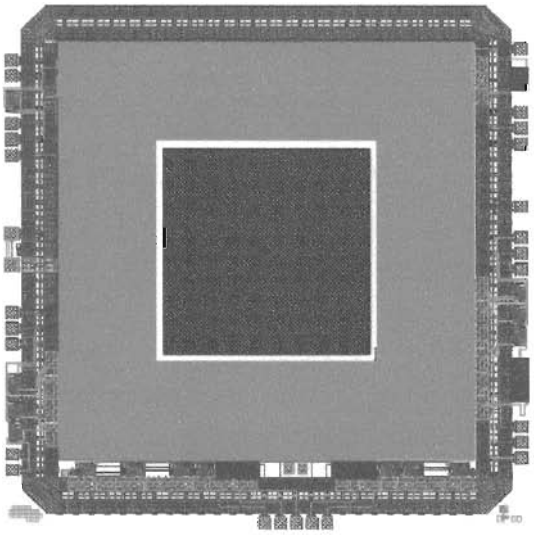

(a) Layout of final chip (3mm x 3mm).

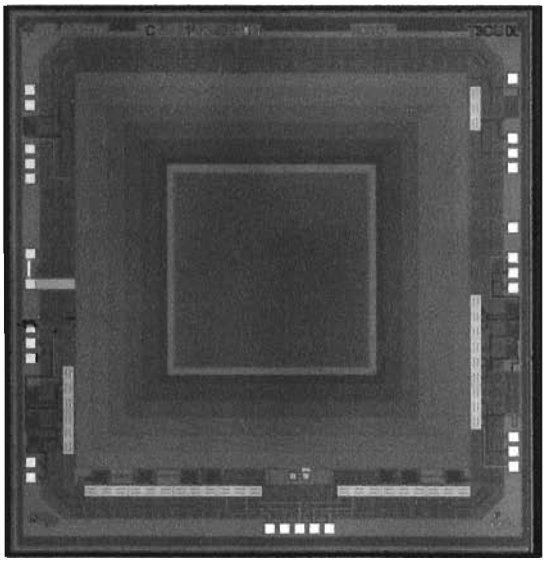

(b) Picture of fabricated chip (3mm x 3mm).

Figure 3.1: Final Chip

Parameter	Description	Value
n	number of turns per metal layer	129
d_{in}	diameter of interior of telecoil	$1270\mu m$
w	line width	$2.7\mu m$
s	line spacing	$1.8\mu m$
t	line thickness	$1\mu m$
m	number of metal layers	2

Table 3.1: Parameters for Equations 3.1-3.7.

turns of the telecoil on one metal layer was used for the value of n. The parameter d_{in} is the diameter of the space inside the telecoil. The parameters w, s, and t are respectively the average width, spacing, and thickness of the metal lines. The number of metal layers is used for the final estimate of the inductance and is defined by the parameter m. The divergence from the parameters in Table 3.1 due to the properties of the via connections between metal layers M1 and M2 are neglected in this calculation.

The total inductance for a single metal layer inductor is the sum of the self inductance L_{self}, and the mutual inductance.The mutual inductance is split into the negative mutual inductance $-M^{-}$, and the positive mutual inductance M^{+}. An estimate for a multiple layer inductor is obtained by multiplying this sum by the parameter m as shown by

$$L_T = m * \left(L_{self} - M^{-} + M^{+}\right) \tag{3.1}$$

$$\tag{3.2}$$

However, this estimate neglects both the positive and negative mutual inductance from metal lines on different metal layers. The value for L_{self} is obtained empirically by

$$L_{self} = \frac{\mu_o}{2\pi} l \left(\ln \frac{l}{n(w+t)} - 0.2\right) \tag{3.3}$$

$$= 1.4165\mu H$$

using the total length of wire l and the parameters n, w and t. The total length of wire on one metal layer is described by

$$\begin{aligned} l &= (4n+1)\left(d_{in} + n(w+s)\right) \\ &= 0.9567m \end{aligned} \tag{3.4}$$

and is estimated from the parameters n, d_{in}, w, and s. The total positive mutual inductance M^+ is described by

$$\begin{aligned} M^+ &= \frac{\mu_o}{2\pi} l(n-1) \ln\left(\sqrt{1+\left(\frac{l}{4nd^+}\right)^2} + \frac{l}{4nd^+}\right) \\ &\quad -\frac{\mu_o}{2\pi} l(n-1)\left(\sqrt{1+\left(\frac{4nd^+}{l}\right)^2} + \frac{4nd^+}{l}\right) \\ &= 50.15\mu H \end{aligned} \tag{3.5}$$

and is dependent on l, n, and d^+. d^+ is the average distance between lines contributing to a positive mutual inductance and is described by

$$\begin{aligned} d^+ &= (w+s)\frac{n+1}{3} \\ &= 195\mu m \end{aligned} \tag{3.6}$$

and is dependent on w, s, and n. The negative mutual inductance M^- is described by

$$
\begin{aligned}
M^{-} &= 0.47\frac{\mu_o}{2\pi}nl \\
&= 11.60\mu H
\end{aligned}
\tag{3.7}
$$

and is dependent on only l and n. Therefore by Equation 3.1, the total inductance L_T is equal to 79.9μH.

The simulated capacitance of the telecoil includes the metal to metal and metal to substrate capacitances and totals $238pF$. This estimate, however, does not take into account interline capacitance. The interline capacitance C_{line} can be estimated by

$$
\begin{aligned}
C_{line} &= \epsilon_{ox}\frac{A}{d} \\
&= m\epsilon_{ox}\frac{lt}{s} \\
&= 36.7pF
\end{aligned}
\tag{3.8}
$$

which is a model of a parallel plate capacitor. The two parallel plates are the vertical sides of the metal lines of the telecoil. Therefore the area A of the metal plates can be defined as lt and s is the distance d between the plates. The parameter m is multiplied since there are multiple layers of the telecoil. The total capacitance of the telecoil C_L is the sum of the simulated capacitance and the interline capacitance and is therefore $238pF + 36.7pF = 275pF$. The metal to metal and metal to substrate capacitances dominate over the interline capacitance.

The top metal layer has an area of $2.58 * 10^6\mu m^2$. The telecoil is so large that it violates antenna rules when connected to the gate of a MOS transistor. Therefore a fuse was created to tie the telecoil to substrate during fabrication. Before testing with an amplifier, the fuse line has to be hand scribed to open the fuse. Figure 3.2 shows the

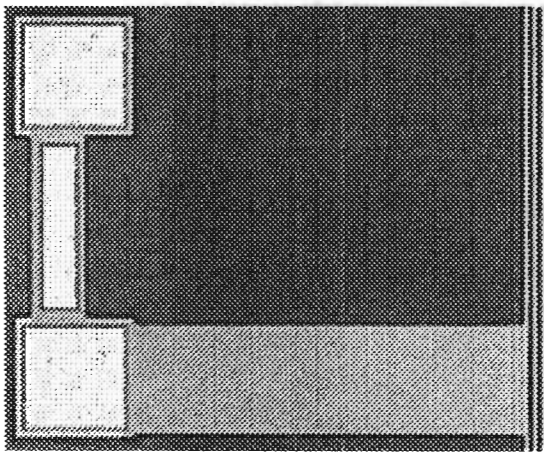

Figure 3.2: Picture of the fabricated fuse.

telecoil fuse layout. There are also probe pads connected to the ends of the telecoil for the direct testing of telecoil parameters.

3.2 Testing

The DC resistance of the telecoil was measured to be $34k\Omega$ which is in good agreement with simulated results. However, because of this high resistance, the precision LCR meter (Agilent 4284A) cannot measure the inductance or capacitance. Therefore, the theoretical values derived in the previous section were used as estimates.

Figure 3.3 shows a diagram of the testing apparatus. A function generator (Agilent 33250A) is connected to the ends of a telephone speaker. The speaker is situated directly above the chip. The telecoil probe pads are connected to the spectral analyzer (Agilent 35670A). Data from the spectral analyzer is captured via GP-IB through Labview. This setup allows direct measurement of the response of the telecoil. The spectral analyzer allows analysis of data despite 60Hz noise.

Appendix A describes the commands used to run the spectral analyzer. Appendix B describes the Labview code that was created to capture the information from the GP-IB port of the spectral analyzer.

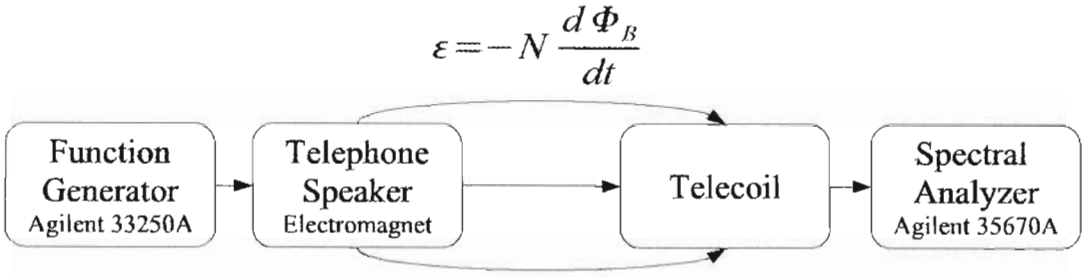

Figure 3.3: Testing apparatus configuration.

The telecoil was tested with three different configurations: the telecoil by itself, the telecoil with a magnetic core situated above, and the telecoil with a permeable (non-magnetic) core situated above. The magnetic core is a neodymium iron boron material with diameter of 0.1 inches and thickness of 0.25 inches[10]. The Curie temperature of this material is 315°C. The permeable core is the same material as the magnetic core but was annealed to 320°C for 10 minutes. After this annealing step, the permeable core no longer exhibited magnetic properties. The experimental setup to test the telecoil is shown in Figure 3.4. The core is placed in the center of and above the integrated telecoil.

Background noise was determined with the experimental setup in Figure 3.3 with zero input to the speaker. This background result was subtracted from the differential voltage signal from the telecoil. Figure 3.5 shows the measured voltage V_T (Equation 2.14) with respect to frequency. In Figure 3.5 the difference in performance between the magnetic and permeable cores actually reverses at higher frequencies. However, at all frequencies the addition of a core increases performance.

Figure 3.6 shows the linearity of the telecoil at 1kHz with a sweep in amplitude of the input signal from 0V to 10V with the speaker located 56mm from the telecoil. Linearity is independent of the type of core used. The graphs should appear linear as the

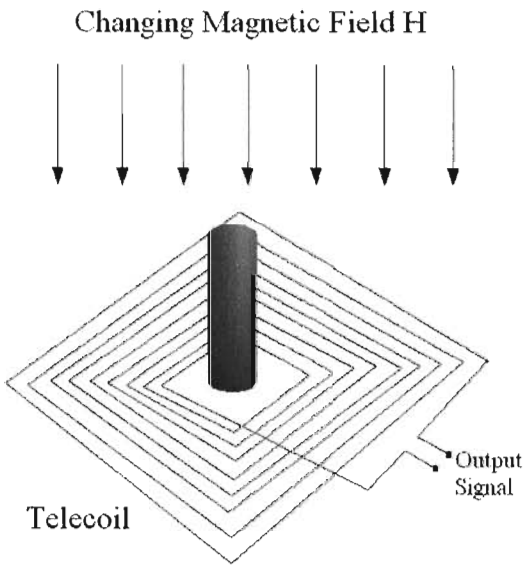

Figure 3.4: Signal from changing magnetic flux.

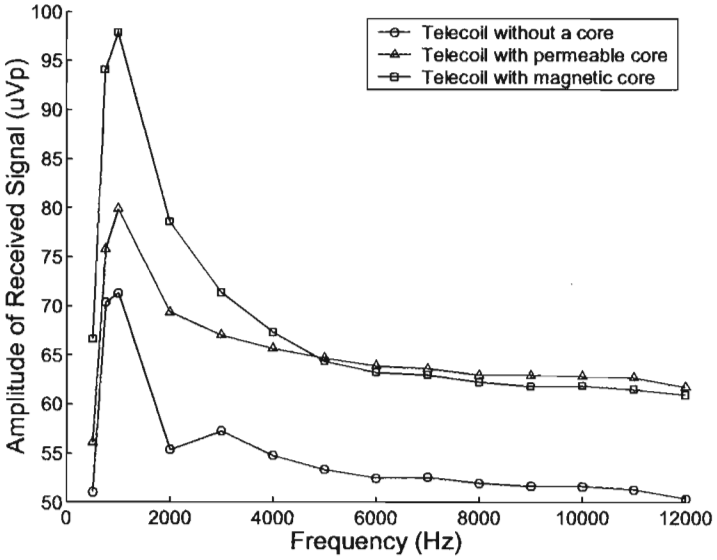

Figure 3.5: Input response of telecoil versus frequency.

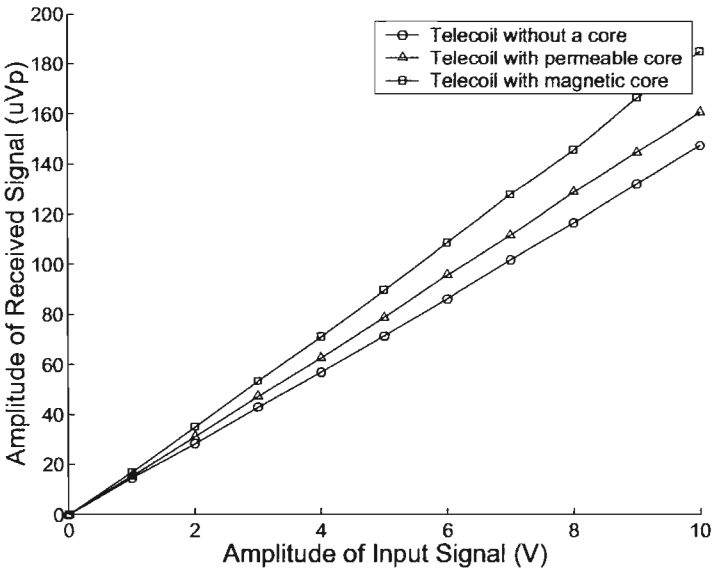

Figure 3.6: Telecoil response vs input amplitude at 1kHz.

telecoil is a passive component. The magnitudes in Figure 3.6 may not be characteristic of the differences between the cores at all frequencies.

There are inductive as well as resistive components to the electromagnet in the telephone speaker and this causes the magnitude of the impedance to be function of frequency. Equation 2.12 describes the voltage over the inductance of the speaker. The value of R_S is 50Ω and the values of R_K and L_K are determined experimentally. Figure 3.7 shows the value of $|Z_K|$ defined by Equation 2.10 using the frequency dependent measured values of R_L and R_K. These values are used to determined emf_k based on a source amplitude of 5V. The result is plotted in Figure 3.8.

The skin depth of a metal such as copper at 20kHz is on the order of 0.5mm. Therefore skin depth should not be affecting either the speaker or the telecoil.

The voltage source V_S shown in Figure 2.2 is not ideal. The power in the signal from the voltage source is mostly in one frequency, but there is a bit of spread to neighboring frequencies. Measured valued of V_T were obtained by integrating over a small range of frequencies near the primary frequency. This works well for frequencies above

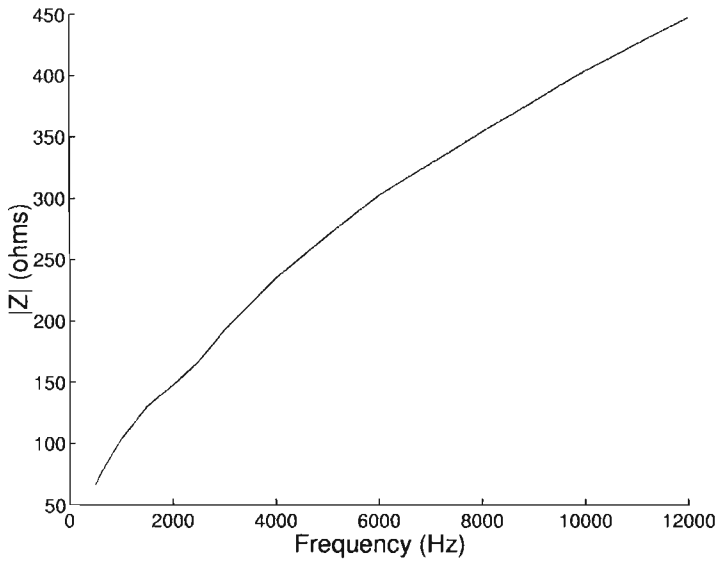

Figure 3.7: Speaker impedance as a function of frequency.

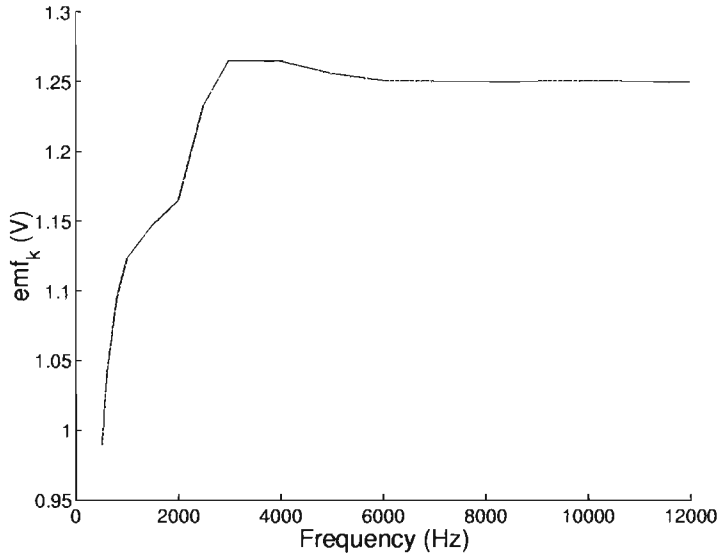

Figure 3.8: emf_k as a function of frequency with V_S of 5V.

1kHz. However, the lower frequencies have a lot of background noise and the amplitude of the noise could have been integrated as well.

The ratio of $\frac{emf_t}{emf_k}$ was obtained using Equation 2.14 and Equation 2.13 and is given by

$$\frac{emf_t}{emf_k} = \frac{|V_T|\,|1 + sR_TC_T|}{|V_S\,\left|\frac{sL_K}{R_K+R_S+sL_K}\right|}. \tag{3.9}$$

Figure 3.9 shows $\frac{emf_t}{emf_k}$ as a function of frequency using the measured values of V_T, R_K, and L_K at each frequency. The amplitude of V_T associated with the lower frequencies is affected by the spread in signal from the function generator. However, at higher frequencies, the value of $\frac{emf_t}{emf_k}$ is independent of frequency. This matches the proposed theory that the frequency dependence of emf_t and emf_k is contained to the parameter K of Equation 2.13 and that M_t and M_k are independent of frequency. The increase in response due to the addition of a permeable core is much lower than expected. The dispersive effects of the magnetic field at the end of the permeable core may account for some of this result. However, more research is needed into the exact cause of this phenomenon.

Figure 3.10 shows the amplitude of the response of the telecoil when the probe pads are worn. Worn probe pads increase the resistance of the connection to the telecoil, and therefore attenuate the received signal. Figure 3.11 shows that the amplitude response is fairly constant when the experimental setup is left undisturbed. Since the results when the experiment is left undisturbed does not change significantly, the degradation in signal amplitude from Figure 3.10 is most likely due to pad degradation and not a reproducibility issue. A recommendation for future research would involve including several sets of probe pads for testing purposes. This would allow testing on a single telecoil with several data sets of the same probe pad conditions.

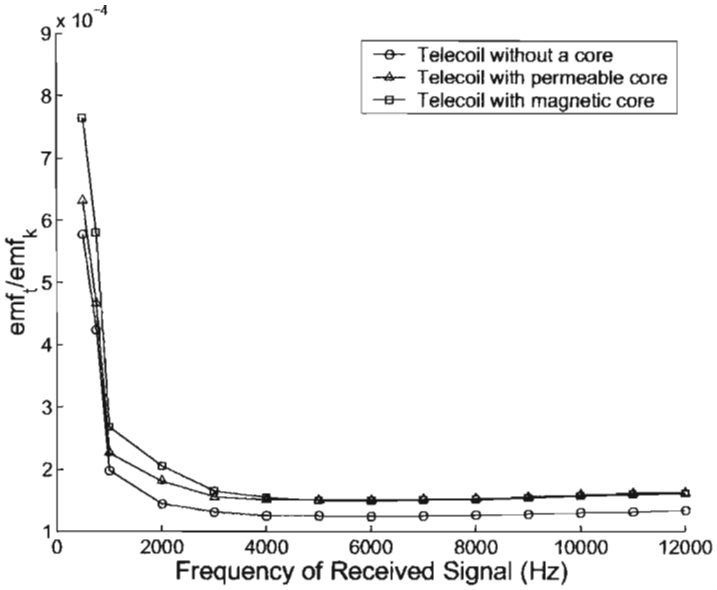

Figure 3.9: Graph of $\frac{emf_t}{emf_k}$ versus frequency.

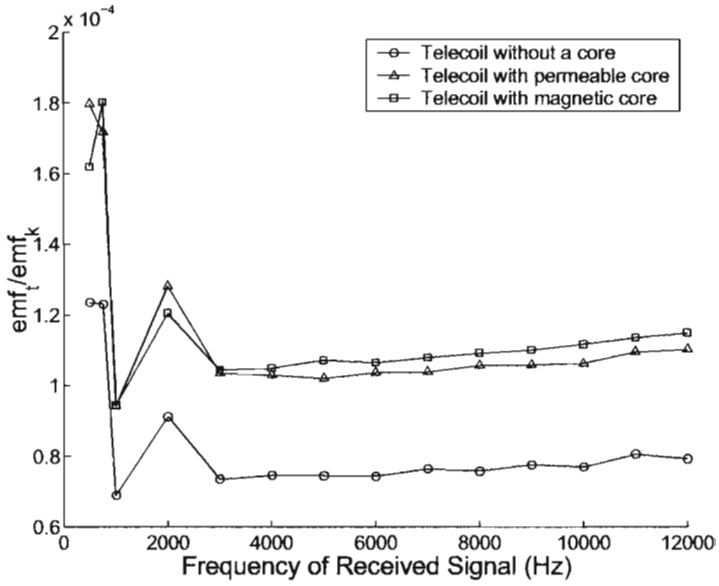

Figure 3.10: $\frac{emf_t}{emf_k}$ of telecoil with worn probe pads.

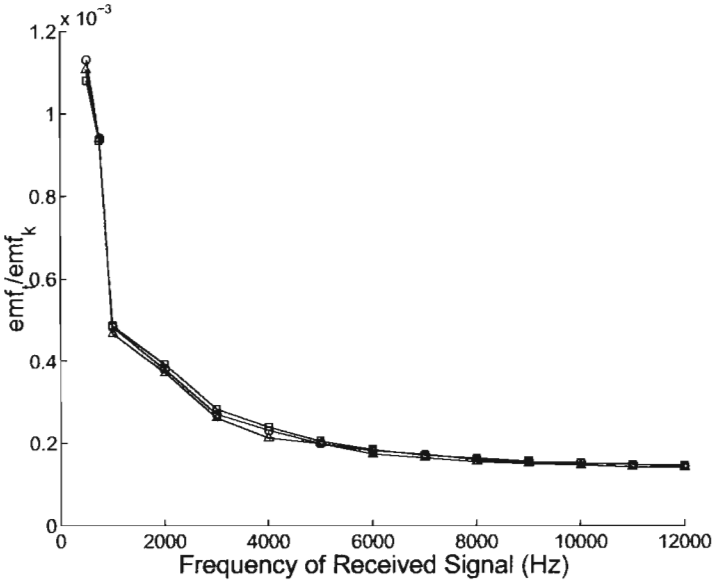

Figure 3.11: Reproducibility of $\frac{emf_t}{emf_k}$ versus frequency over time (no core).

Figure 3.12 shows that the magnitude of the telecoil signal is of the form $A + \frac{B}{r^3}$ where A equals 69.6, B equals $1.62 * 10^7$ and r is the distance between the speaker and telecoil. The theory as shown in Equation 2.8 expects a $\frac{1}{r^3}$ dependence. More research is needed to determine the cause of this discrepancy.

3.3 Summary

The integrated telecoil acts as a magnetic flux sensor by picking up the magnetic signal from the phone speaker. Figure 3.13 shows that the integrated telecoil is smaller than commercially available telecoils, which may allow telecoils to be available in all types of hearing aids.

Neglecting the noise associated with lower frequencies, it is shown in Figure 3.9 that the telecoil response is not dependent on frequency which agrees with theory described by Equation 2.13. Figure 3.12 shows that the magnitude of the telecoil is of the form of $A + \frac{B}{r^3}$ where A equals 69.6 and B equals $1.62 * 10^7$. This result differs

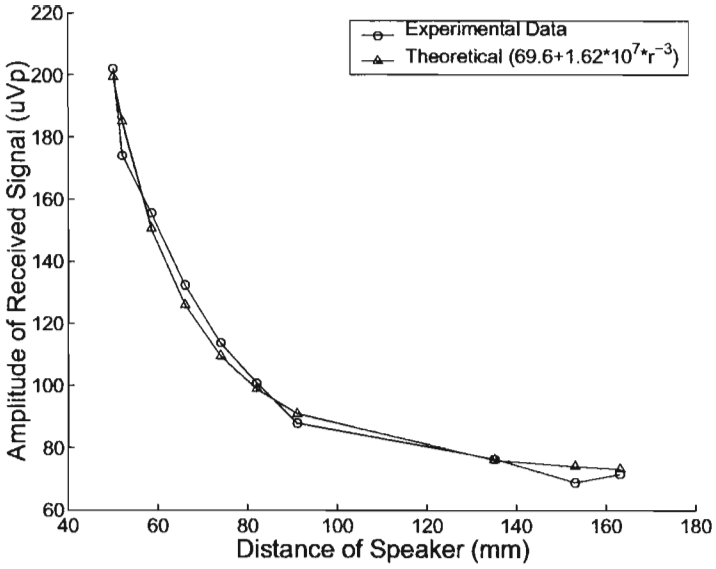

Figure 3.12: Received signal amplitude vs distance of speaker.

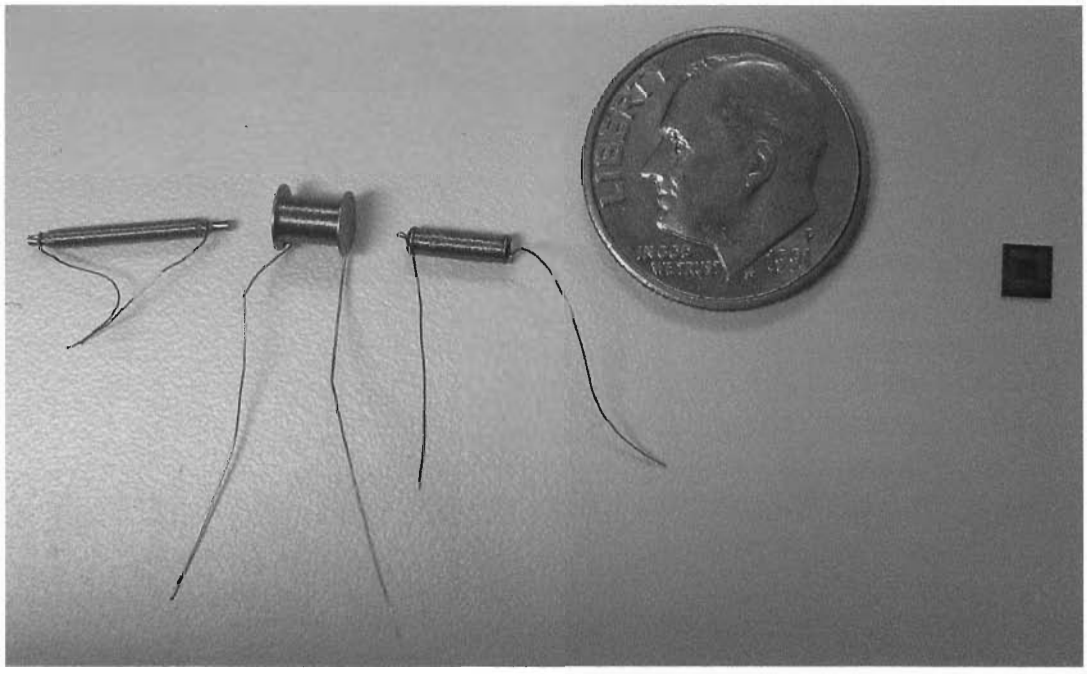

Figure 3.13: Example size of several commercial telecoils (left) and the integrated telecoil (right).

from the theory defined in Equation 2.8. The increase in response due to the addition of a permeable core is much lower than expected. The dispersive effects of the magnetic field at the end of the permeable core may account for some of this result. However, more research is needed into the exact cause of this phenomenon.

Possible improvements for the future include extending the telecoil into a process with 6 or more metal layers. This will greatly increase the number of turns possible and therefore increase the voltage signal from the telecoil. It would also be beneficial to fabricate several telecoils with different line widths to control resistance and investigate the effects of resistance, capacitance and inductance. The resistance of the telecoil was a large obstacle in experimentally finding the C_T and L_T of the telecoil. The precision LCR meter could not determine those parameters of a circuit due to the magnitude of R_T. Several sets of probe pads on the telecoil would allow more data to be taken per fabricated telecoil.

Eventually it would be ideal to deposit the permeable core directly onto the silicon substrate. Magnetic materials have previously been deposited for use as printing heads[11] and therefore it could possibly be extending to non-magnetic permeable materials as well. The neodymium iron boron core used for testing has a low Curie temperature of $315°C$ and would therefore be demagnetized during regular semiconductor fabrication.

CHAPTER 4

AMPLIFIER DESIGN

4.1 Cherry Hooper Design

This section describes an integrated circuit with two fully differentiable amplifiers attached to a telecoil. The two amplifiers connected to the telecoil are static gain amplifiers. To offset this liability, they have different gain regions. Several test amplifiers are included to characterize the performance of the amplifier configuration as well as test structures for the main design in case unexpected behavior was observed.

4.1.1 Circuit Design

The Cherry Hooper amplifier design [12] is a commonly used transconductance to transimpedance amplifier designed to work with very small input signals. Figure 4.1 shows that the single Cherry Hooper stage actually consists of a two stage fully differential amplifier with passive feedback. A simple current mirror was used for the current source. Iterative parametric simulations were used to obtain the optimum configuration for gain performance while minimizing total harmonic distortion (THD) and noise analysis for the 0.5μm AMI CMOS process. The values used for the components in this design are shown in Table 4.1. The resistances and transistors need to be matched which requires special layout considerations such as a common centroid layout.

The design consists of a three stage amplifier and a four stage amplifier connected to the telecoil and with filters. Both of these amplifier designs include a low-pass filter. Several test circuits also exist including a stand-alone three stage amplifier with filter, a three stage amplifier without filter, a single stage amplifier, and a test filter. These will

allow accurate debugging in the case of circuit failure. However, due to layout restrictions, complete simulations were only completed for the single stage test amplifier, and three stage test amplifier with filter.

The output filter consists of a simple low-pass RC filter. It has an RC time constant of 25μs and consists of a resistor of 5MΩ and a capacitor of 5pF.

4.1.2 Circuit Performance

All the circuit simulations were performed at 37.78°C. This is slightly greater than body temperature and is close to the operating temperature of a hearing aid. The input signal has a frequency of 1kHz and a peak to peak amplitude of 1μV unless otherwise noted. The signal from the telecoil had been estimated as 1μV

The output from the single stage amplifier has a bias voltage of 1.88V. If this signal was attached to the next stage of a multiple stage amplifier, the outputs of the second stage would saturate. This dc offset voltage is too high for identical stages to be directly coupled. Therefore, decoupling capacitors of 5pF are added differentially between stages to bring the common mode voltage to zero for the following stage inputs.

Figure 4.2 shows the gain response of a single stage Cherry Hooper amplifier as a function of input signal peak to peak amplitude. The circuit provides 27dB of gain up to a 10mV input signal before starting to saturate.

Parameter	Value
Rd	850Ω
Rf	6.5kΩ
$\left(\frac{W}{L}\right)_{M0,1,2,3}$	$\frac{300\mu m}{0.6\mu m}$
Vdd	2.5 V
Vss	-2.5 V
Is	827μA

Table 4.1: Parameters for circuit shown in Figure 4.1.

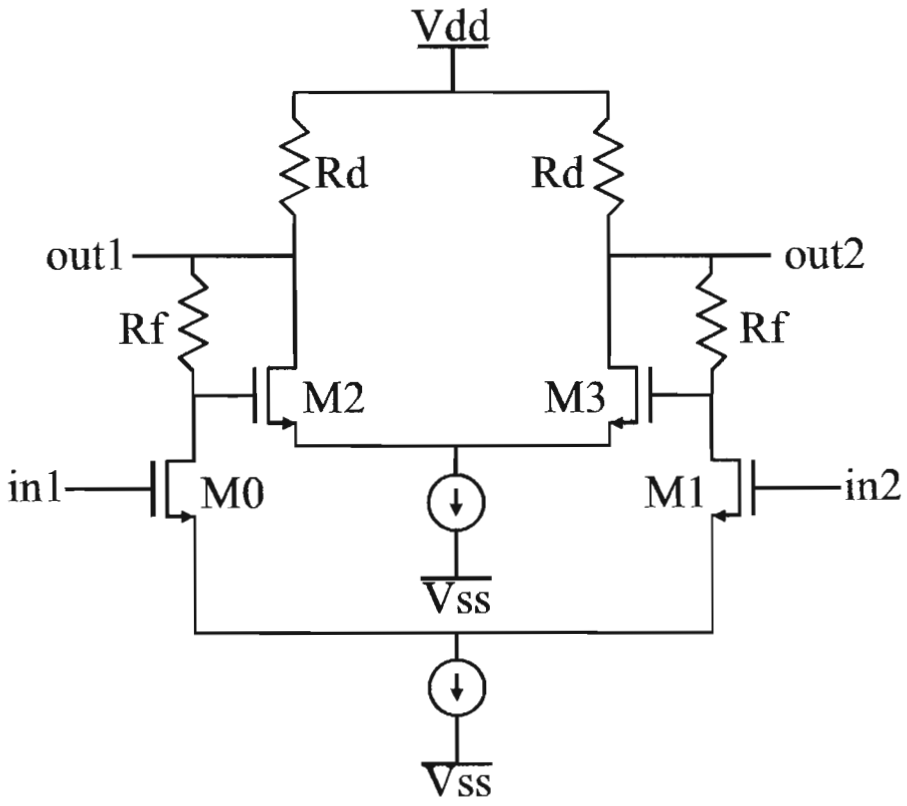

Figure 4.1: Cherry Hooper amplifier schematic.

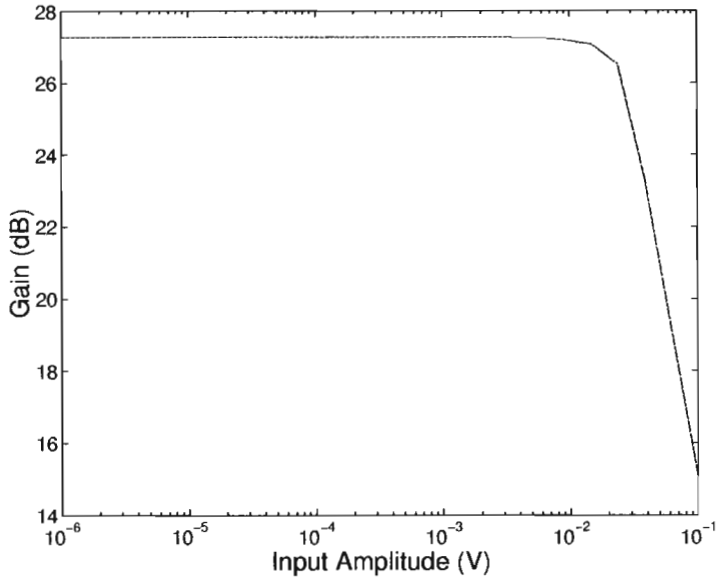

Figure 4.2: Single stage Cherry Hooper gain response.

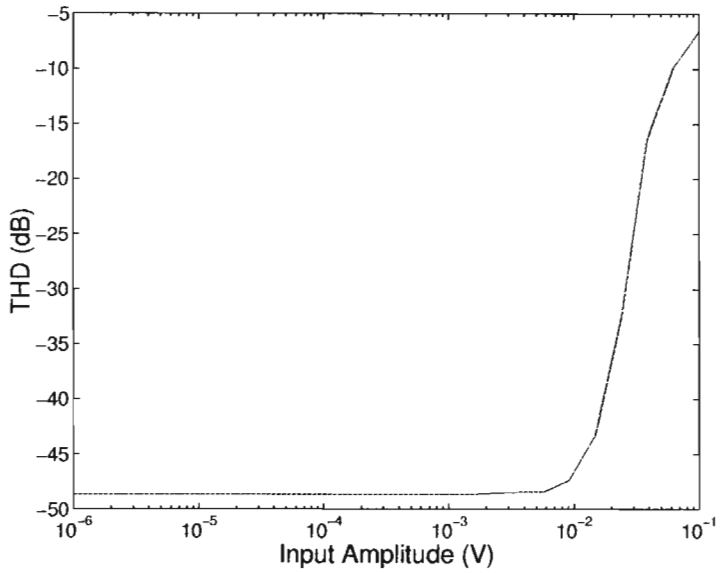

Figure 4.3: Single stage Cherry Hooper THD response.

Figure 4.3 shows that the THD response of the single stage Cherry Hooper amplifier is -49dB for inputs up to 10mV.

The three stage amplifier with filter design was analyzed with worst case pins of the package model DIP40 attached to the outputs. The three stage Cherry Hooper amplifier design uses three identical single stage blocks with decoupling capacitors between stages and a filter on the output. There are no decoupling capacitors on the output of the three stage amplifier, so therefore there is a final output bias of 1.88V shown in Figure 4.4.

Figure 4.5 shows that the THD response of the three stage Cherry Hooper amplifier is approximately -50dB for inputs up to 10μV, which is acceptable for hearing aid applications.

Figure 4.6 shows the three stage Cherry Hooper amplifier gain to be $85dB$. This circuit is linear for input amplitudes up to $10\mu V$.

The AC response of the three stage amplifier with filter in Figure 4.7 shows that the 3dB point is at 3kHz, which will eliminate the high frequency noise on the output.

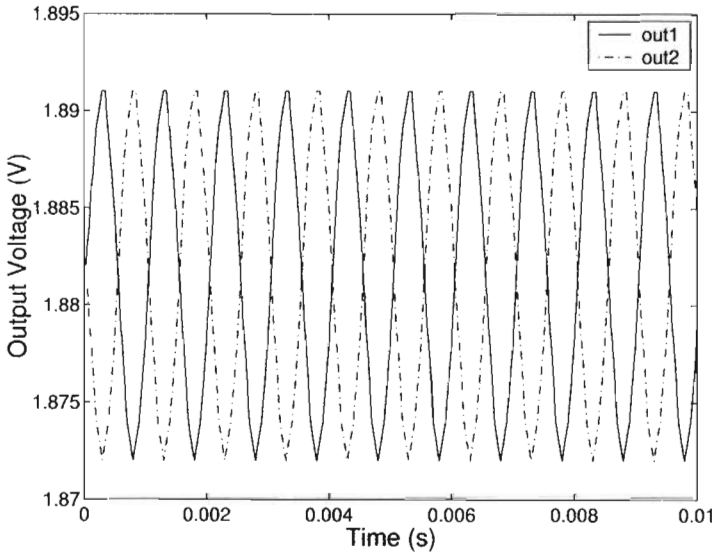

Figure 4.4: Three stage Cherry Hooper with filter biasing.

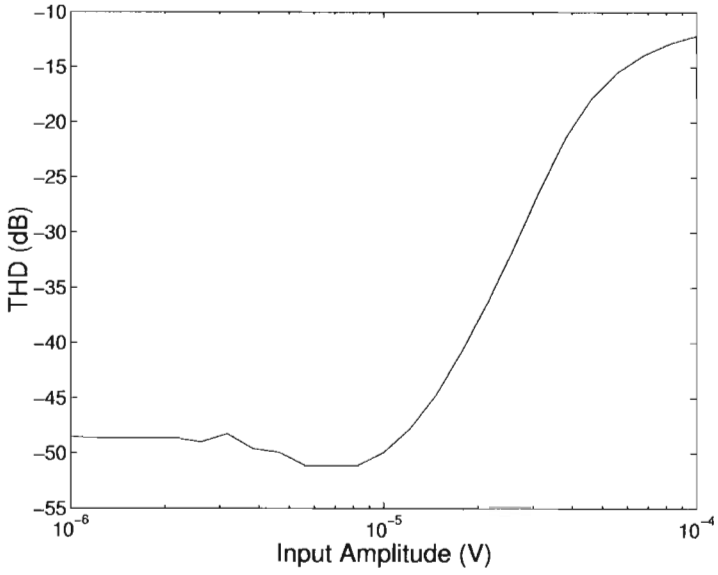

Figure 4.5: Three stage Cherry Hooper with filter THD response.

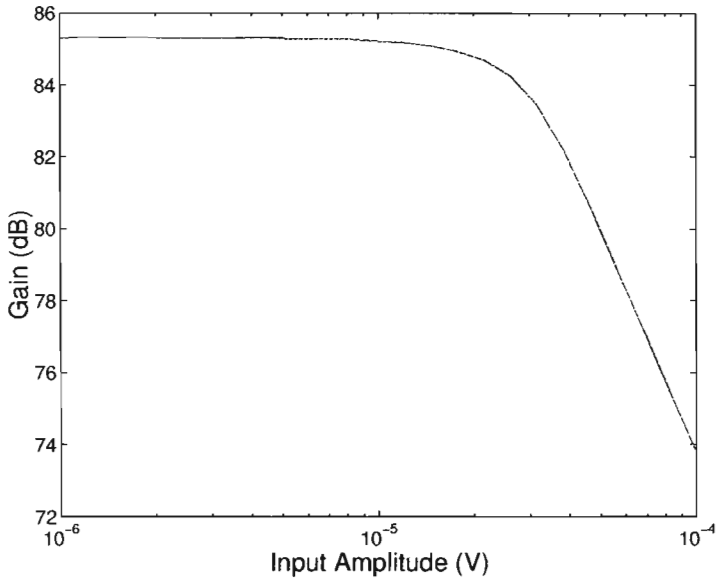

Figure 4.6: Three stage Cherry Hooper with filter gain response.

This value is not the perfect choice for a hearing aid application which should not start attenuation until frequencies reach 5kHz or more. However, for this project the filter is sufficient and most of the testing will be done at 1kHz, which is not attenuated.

Table 4.2 shows the equivalent input noise of the different Cherry Hooper amplifiers. The noise of the single stage amplifier is $2.014\frac{nV}{\sqrt{Hz}}$. Over a frequency range of 10kHz, this would result in noise of about $0.2\mu V$. The input noise of the three stage Cherry Hooper amplifier is $2.016\frac{nV}{\sqrt{Hz}}$, which is only slightly greater than the single stage noise.

Figure 4.8 shows the gain of the three stage amplifier as a function of decoupling capacitance. There is negligible attenuation for the signal if the decoupling capacitor is

Amplifier	Input Referred Noise $\left(\frac{nV}{sqrtHz}\right)$
SS Cherry Hooper	2.014
3S Cherry Hooper	2.016

Table 4.2: Input referred noise for Cherry Hooper amplifier.

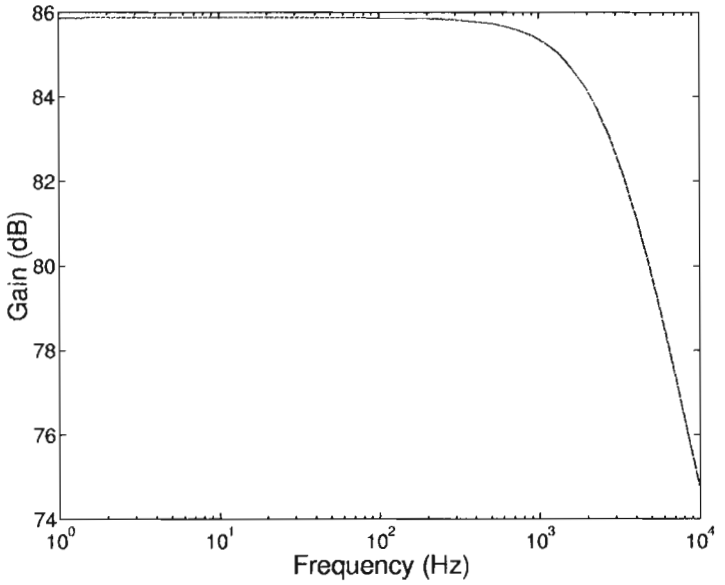

Figure 4.7: Three stage Cherry Hooper amplifier with filter AC response.

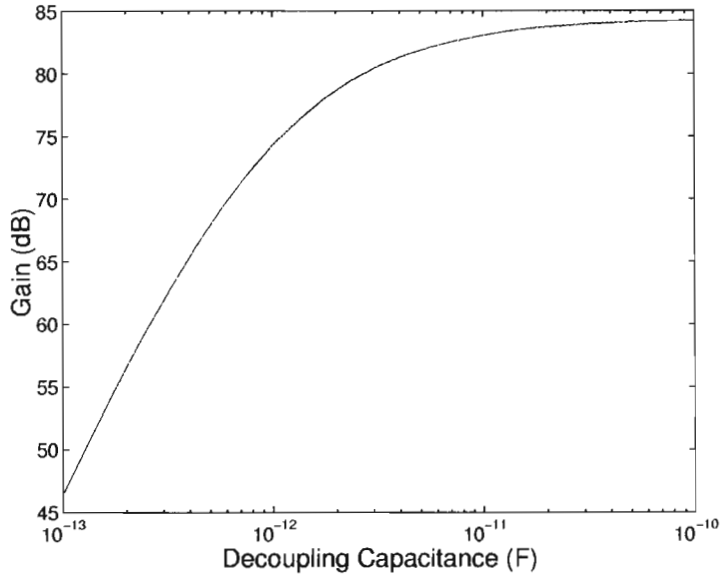

Figure 4.8: Decoupling capacitance between stages.

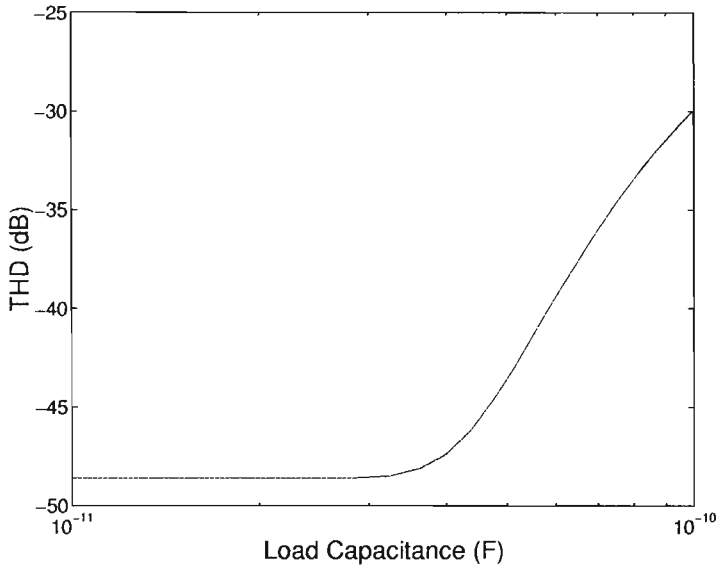

Figure 4.9: Capacitance drive capability of three stage Cherry Hooper amplifier with filter.

$10pF$ or greater. The tradeoff in this case is between layout size of the decoupling capacitors and overall gain performance of the amplifier. The value of $5pF$ was chosen to balance these two tradeoffs.

Figure 4.9 shows that no output buffer is needed on the circuit. The three stage amplifier with filter and worse case pins can drive an additional capacitance load of $30pF$ without sacrificing THD performance. The capacitance for the testing equipment for this project should be less than $30pF$.

4.1.3 Physical Design

Figure 4.10 shows the layout of the single stage Cherry Hooper amplifier. This design uses the common centroid layout design to minimize variations in parasitics in matched transistors. The multiple stage amplifiers consist of several single stage blocks with the decoupling capacitors in between stages. The pinout and bonding diagram for this design are found in Appendix C.

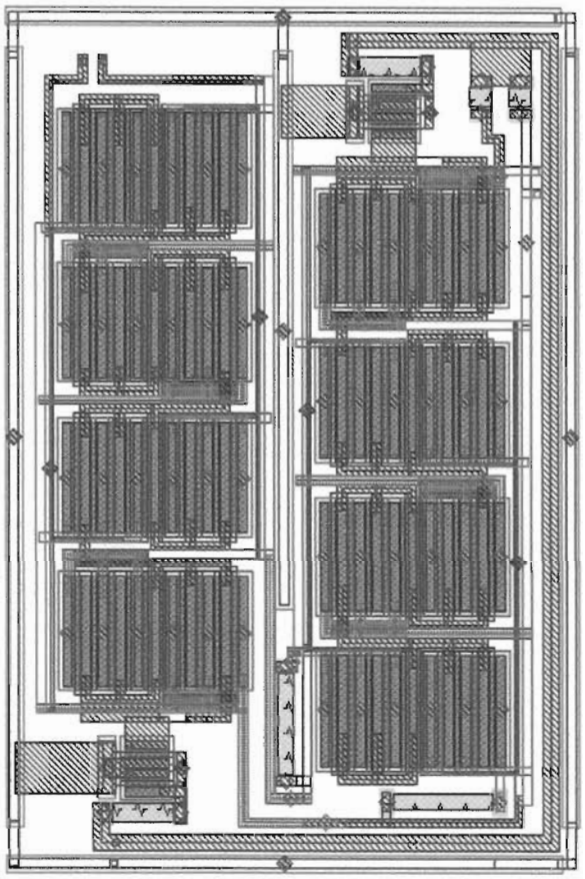

Figure 4.10: Cherry Hooper amplifier layout.

The main disadvantage of this design is that it does not scale to lower voltages[15] found in hearing aid applications.

4.1.4 Experimental Results

With a test input signal amplitude of 1mV, the gain of the single stage test amplifier was measured to be 18dB, which is much lower than the expected 27dB. The three stage and four stage amplifiers attached to the telecoil as well as the three stage test amplifier attenuate the input signal down to zero. More time and research are needed to find out what exactly affected the gain of the Cherry Hooper amplifiers.

4.2 Single Ended Amplifier

The design of a second amplifier using a two stage single-ended amplifier configuration was investigated. This amplifier uses a low-noise preamplifier and then a larger gain second stage. The test chip which is fabricated consists of the preamplifier and the complete single-ended amplifier connected to the telecoil, as well as test amplifier circuits which operate from separate power sources.

4.2.1 Circuit Design

The preamplifier was modified from a bipolar circuit [13] and is shown in Figure 4.11. This transimpedance amplifier consists of two common source stages in cascade and a current follower. The common source stages are implemented by transistors M0 and M3, while the current follower is implemented by transistors M1 and M2. Transistors M4, M5, and M6 as well as the resistor R_s define the bias circuitry. The resistor R_f is used adjust the gain of the amplifier. This circuit is scalable for low-voltage applications and constitutes the low-voltage counterpart of a common gate stage[1]. The current source is biased to provide $770\mu A$. The values of the device parameters are given in Table 4.3.

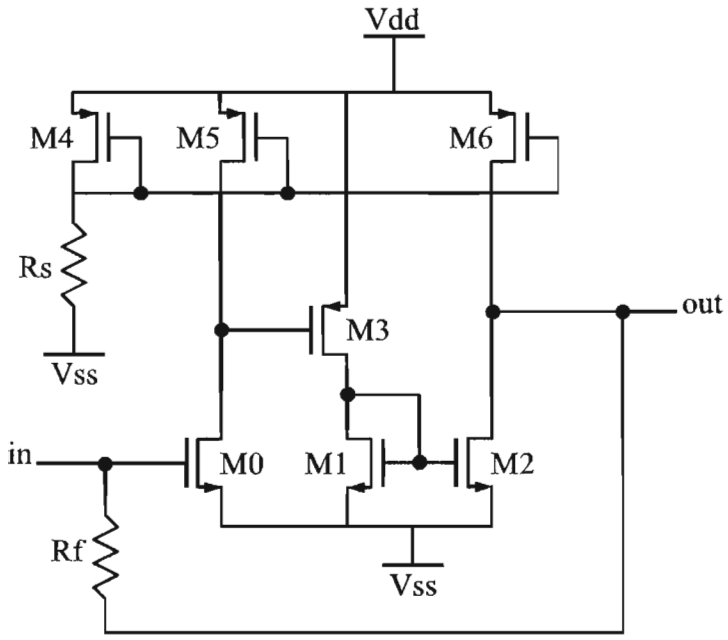

Figure 4.11: Circuit diagram of preamplifier.

Parameter	Value
R_s	$2.8k\Omega$
R_f	$30k\Omega$
$\left(\frac{W}{L}\right)_{M0,1,2}$	$\frac{5.25\mu m}{1.05\mu m}$
$\left(\frac{W}{L}\right)_{M3,4,5,6}$	$\frac{16.8\mu m}{1.05\mu m}$

Table 4.3: Parameters for circuit shown in Figure 4.11.

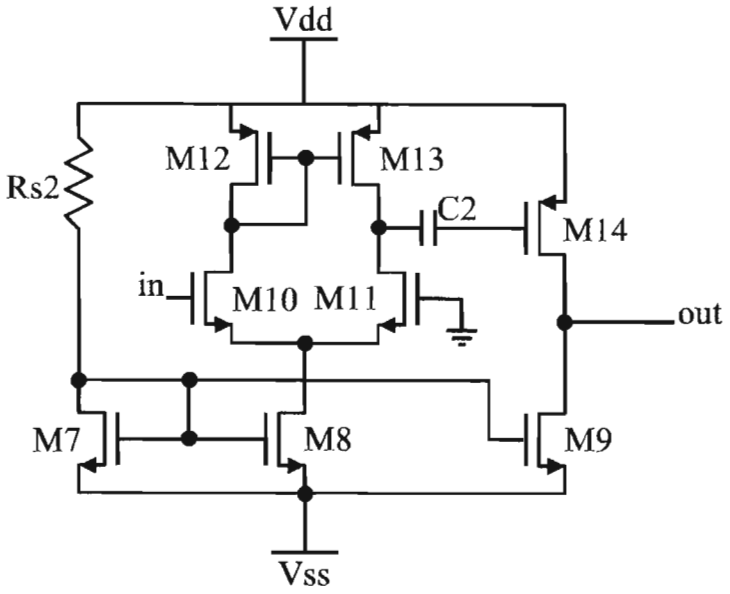

Figure 4.12: Circuit diagram of second stage of amplifier.

Figure 4.12 shows the schematic diagram of the second stage of the amplifier which was modified from a basic operational amplifier design[14]. This differential amplifier has one end tied to ground for single-ended use. It has an active current mirror load and an output buffer. The capacitor C_2 is used to decouple the signal between stages. The transistors M10 and M11 form the differential pair with transistors M12 and M13 forming the active load and M14 the output buffer. The transistors M7, M8 and M9 as well as the resistor R_{s2} form the biasing for this stage. The current source is biased to provide $570\mu A$ and the gain of the second stage is very dependent on the value of the current. The values of the device parameters are found in Table 4.4.

Figure 4.13 shows the schematic of the complete amplifier. Capacitor C_1 is used as a decoupling capacitor and has the same value as capacitor C_2 for convenience.

4.2.2 Circuit Performance

Unless stated otherwise, all simulations were done with an voltage amplitude of 1μA, a frequency of 1kHz, a temperature of 27$\circ$C, and a 40pF load capacitance.

Parameter	Value
R_{s2}	$4k\Omega$
C_2	$5pF$
$\left(\frac{W}{L}\right)_{M7,8,9,10,11}$	$\frac{5.25\mu m}{1.05\mu m}$
$\left(\frac{W}{L}\right)_{M12,13,14}$	$\frac{16.8\mu m}{1.05\mu m}$

Table 4.4: Parameters for circuit shown in Figure 4.12.

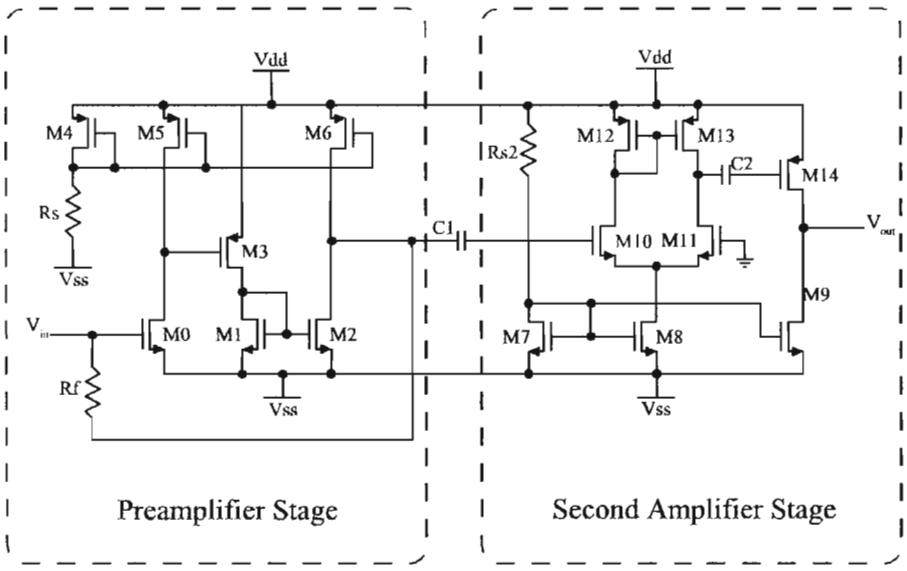

Figure 4.13: Circuit diagram of complete single-ended amplifier.

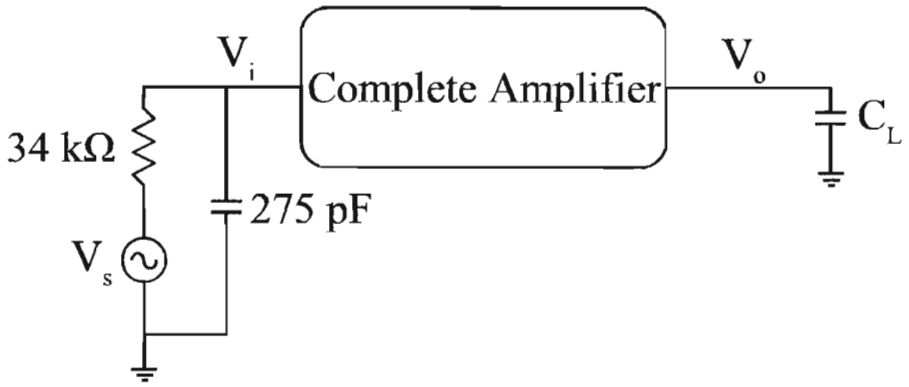

Figure 4.14: Simulation setup for single-ended amplifier and preamplifier.

The preamplifier is a transimpedance amplifier and therefore the voltage gain characteristics were only simulated for the complete amplifier. Figure 4.14 shows the simulation setup used for the following analysis, which is based upon the model for the telecoil shown in Figure 2.2. The gain of the complete amplifier is defined as $\frac{V_{out}}{V_{in}}$.

Figure 4.15 shows the gain versus frequency response of the complete single-ended amplifier. The 3dB point of the amplifier is 200kHz, which is above the human range of hearing by a factor of 10.

Figure 4.16 shows the THD performance of the complete single-ended amplifier to be -48dB. The maximum recommended input amplitude should be 20μV. The input referred noise for the complete amplifier is $45.3\frac{nV}{\sqrt{Hz}}$. This noise value is much higher than the noise of the Cherry Hooper amplifier, but is acceptable.

Figure 4.17 shows that the complete amplifier is capable of driving a load capacitance of $1nF$ with negligible change in gain. The pins of the package used for the device has an estimated capacitance of 40pF. Therefore, this amplifier should have no trouble driving the pin capacitance.

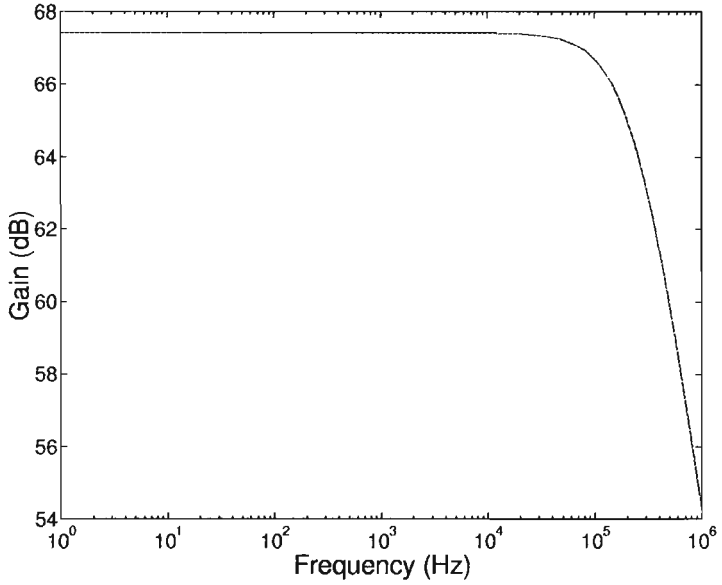

Figure 4.15: Gain response of complete single-ended amplifier .

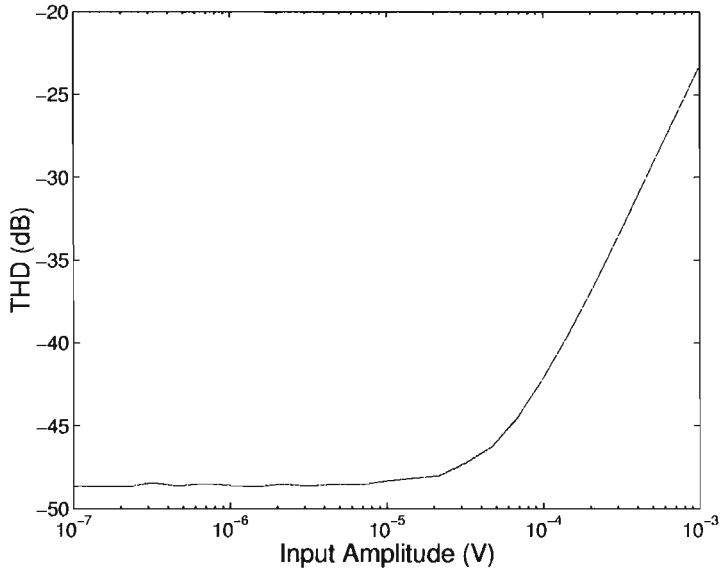

Figure 4.16: THD of complete single-ended amplifier.

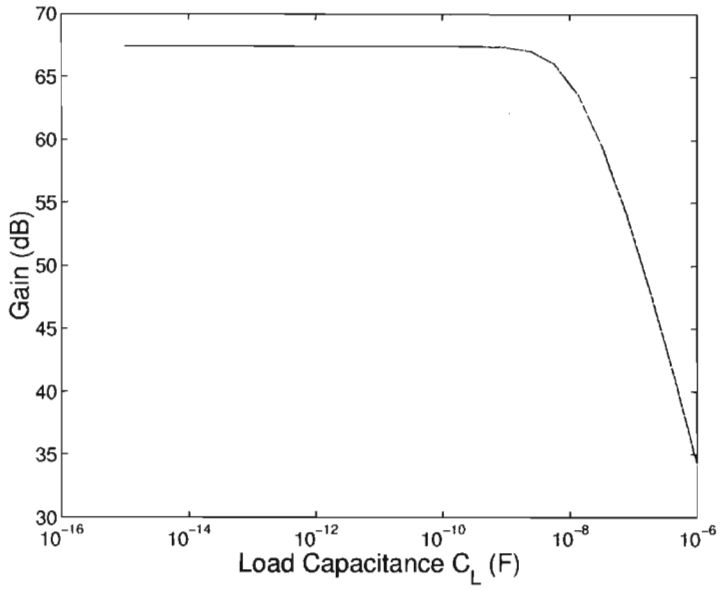

Figure 4.17: Single-ended amplifier with load capacitance.

4.2.3 Physical Design

The process used for fabrication of this design was the 0.5μm AMI CMOS process. Figure 4.18 shows the layout for the preamplifier while Figure 4.19 shows the layout for the second stage amplifier. This design includes a precision resistor implemented in the second level polysilicon. This was implemented because the gain of this stage is very dependent on the current biasing. Figure 4.20 shows the layout for the complete single ended amplifier. Both the layouts for the preamplifier and the second stage amplifier were done to conserve space as well as reduce parasitic capacitances and resistances.

Figure 4.21 shows the layout for the complete test chip. The pinout and bonding diagram for this chip can be found in Appendix C.

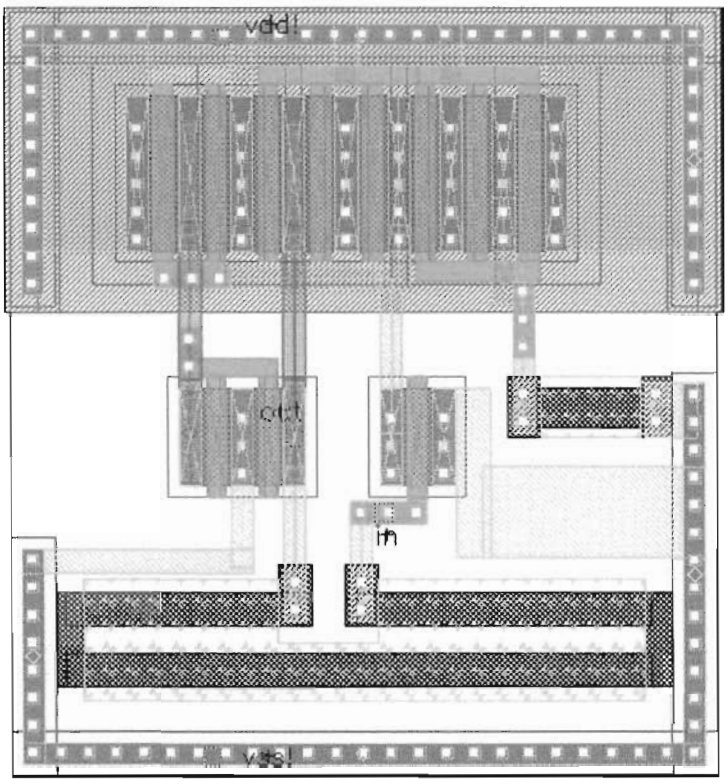

Figure 4.18: Layout of preamplifier

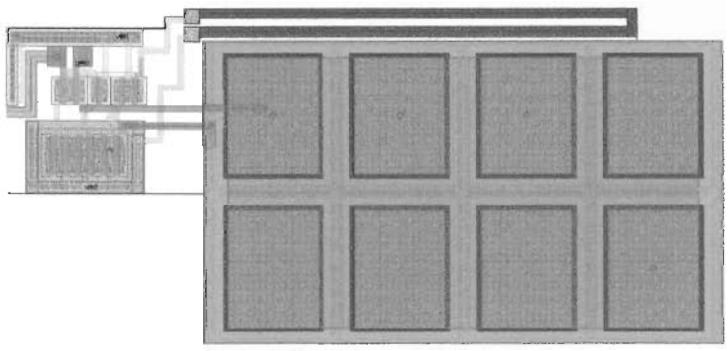

Figure 4.19: Layout of second stage of single-ended amplifier.

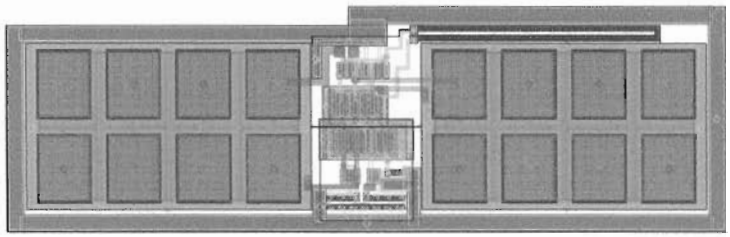

Figure 4.20: Layout of complete single-ended amplifier.

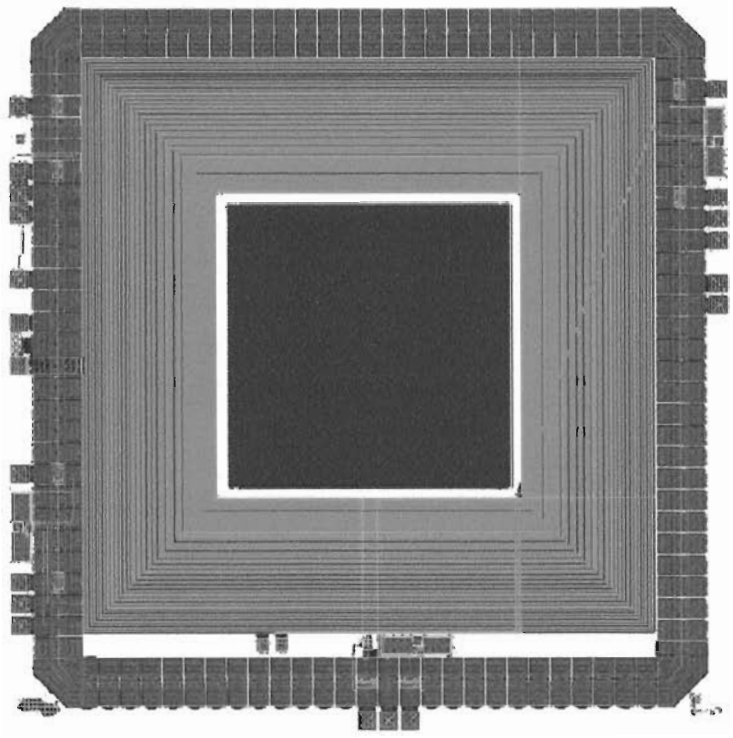

Figure 4.21: Layout of complete design.

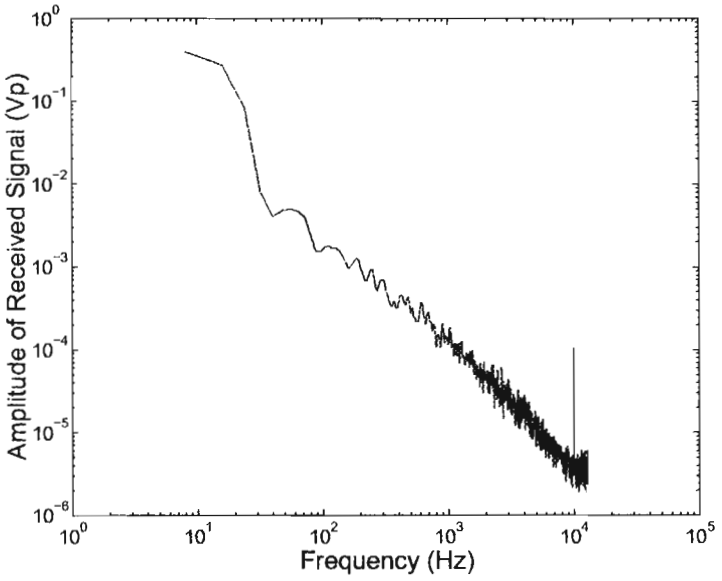

Figure 4.22: Preliminary result showing the output from integrated telecoil and amplifier.

4.2.4 Experimental Results

Unfortunately, the fabricated chips were delayed in processing and did not return in time to do a detailed analysis. Preliminary results of the output response of the telecoil/amplifier combination is shown in Figure 4.22. This signal was obtained with an input voltage of 5Vp on the phone speaker input at a frequency of 10kHz. The speaker and telecoil were separated by 56mm. The peak seen in the figure is at 10kHz and this result demonstrates that the amplifier is functioning with the telecoil as an input.

Unfortunately, this amplifier was designed before detailed experimental results of the telecoil were obtained. Originally, the expected output of the telecoil was 1μV. As seen from Figure 3.9, the output is much greater than the expected 1μV. Therefore, the lack of amplification of the signal may be due to the design of the amplifier for a lower input signal. The input signal amplitude could be lowered from 5Vp, but the background noise is higher than expected and the signal gets lost in the background noise at lower input amplitudes. More research is needed for analysis of the amplifier

to determine the cause of low amplification of the amplifier as well as fully characterize the integrated telecoil and amplifier circuit.

CHAPTER 5

CONCLUSIONS AND FUTURE WORK

A 3-D microelectronic inductor has been fabricated and characterized for use as a magnetic flux sensor, also known as a telecoil, for a hearing aid application. This telecoil was fabricated in a 0.5μm CMOS process with three metal layers, consists of 258 turns each with an average width of 2.7μm and a total wire length of 1.9m. The telecoil has a total area 5.9mm^2 and is situated on a silicon die of 9mm^2. The 3-D structure is more space efficient than conventional spiral inductors and allows for an optimal number of turns for the space available. The telecoil has an inductance of 80μH, a resistance of 34kΩ, and a capacitance of 275pF.

A single stage Cherry Hooper amplifier design was simulated at a gain of 29 dB, THD of -50dB, and equivalent input noise of $2.01\frac{nV}{\sqrt{Hz}}$. The three stage Cherry Hooper design with filter has a simulated gain of 84 dB, THD of -49dB, and equivalent input noise of $2.01\frac{nV}{\sqrt{Hz}}$. The three stage amplifier also has a bandwidth of 3kHz and a driving capacity of 30pF external load capacitance.

The complete single-ended amplifier design was simulated at a gain of 67dB, THD of -48dB, equivalent input noise of $45.3\frac{nV}{\sqrt{Hz}}$, and driving capacity of 1nF external load capacitance.

The integrated telecoil acts as a magnetic flux sensor by picking up the magnetic signal from the phone speaker. The integrated telecoil is smaller than commercially available telecoils, which may allow telecoils to be available in all types of hearing aids.

Neglecting the noise associated with lower frequencies, it is shown that the telecoil response is not dependent on frequency which agrees with theory. The magnitude of the telecoil is of the form of $A + \frac{B}{r^3}$ where r is the distance between the speaker and the telecoil, which differs from the theory. More research is needed to investigate the cause of this discrepancy. The increase in response due to the addition of a permeable

core is much lower than expected. The dispersive effects of the magnetic field at the end of the permeable core may account for some of this result. However, more research is needed into the exact cause of this phenomenon.

Unfortunately, the testing results of the Cherry Hooper amplifier were less than satisfactory. With a test input signal amplitude of 1mV, the gain of the single stage test amplifier is 18dB, which is much lower than the expected 27dB. The three stage amplifier and four stage amplifier attenuate the input signal down to zero. More time and research would need to be invested to find out what exactly affected the gain of the Cherry Hooper amplifiers.

One possible limitation of the Cherry Hooper amplifier is that there is no common mode feedback in the design. If this was part of the design, the decoupling capacitors would not be needed and the amplifier would increase in stability. Another limitation of the Cherry Hooper amplifier is that it does not perform well with a low source voltage[15] which is required for a hearing aid application.

Preliminary analysis of the single ended amplifier was obtained with an input voltage of 5Vp on the phone speaker input at a frequency of 10kHz. The peak seen in Figure 4.22 is at 10kHz and therefore the amplifier was not damaged during fabricated by being connected to the telecoil. The lack of amplification of the signal may be due to the design of the amplifier for a lower input signal. More research is needed for analysis of the amplifier to determine the cause of low amplification of the amplifier.

Possible improvements for the future include extending the telecoil into a process with 6 metal layers. This will greatly increase the number of turns possible and therefore increase the voltage signal from the telecoil. It would also be beneficial to fabricate several telecoils with different line widths. The resistance of the telecoil was a large obstacle in experimentally finding the C_T and L_T of the telecoil. The precision LCR meter could not determine those parameters of a circuit due to the magnitude of R_T.

It would also be beneficial for the amplifier to be variable gain[16] to allow consumer adjustment of volume.

An accurate bandpass filter would be beneficial to eliminate noise coming from frequencies outside the range of human hearing. A combination of second order Butterworth filters have previously been implemented in integrated hearing aid circuitry[1] and could be applied to this application as well.

Eventually it would be ideal to deposit the permeable core directly onto the silicon substrate. Magnetic materials have previously been deposited for use as printing heads[11] and therefore it could possibly be extending to non-magnetic permeable materials as well. The neodymium iron boron core used for testing has a low Curie temperature of 315°C and would therefore be demagnetized during regular semiconductor fabrication.

REFERENCES

[1] W. A. Serdijn, *The design of Low-Voltage Low-Power Analog Integrated Circuits and their Applications in Hearing Instruments*. PhD thesis, Delft University, Stevinweg 1, 2628 CN Delft, The Netherlands, February 1994.

[2] http://www.hearingloop.org/, "HearingLoop: Getting hard of hearing people 'in the loop'." World Wide Web, April 2004.

[3] http://www.shhh.org/, "Shhh: The nation's voice for people with hearing loss." World Wide Web, April 2004.

[4] http://www.hear it.org/, "Hear-it: Hearing, hearing loss and hearing aids - your ultimate source." World Wide Web, December 2003.

[5] B. F. Marshall and M. A. Craig, "Inductive device." Patent Application: US 6819213 B2, November 2004.

[6] R. K. Wangsness, *Electromagnetic Fields*. John Wiley and Sons, Inc., 2 ed., 1986.

[7] H. D. Young and R. A. Freedman, *University Physics*. Addison-Wesley Publishig Company, Inc, 9 ed., 1996.

[8] C.-C. Tang, C.-H. Wu, and S.-I. Liu, "Miniature 3-D inductors in standard CMOS process," *IEEE Journal of Solid-State Circuits*, vol. 37, pp. 471–480, April 2002.

[9] S. Jenei, B. K. J. C. Nauwelaers, and S. Decoutere, "Physics-based closed-form inductance expression for compact modeling of integrated spiral inductors," *IEEE Journal of Solid-State Circuits*, vol. 37, pp. 77–80, January 2002.

[10] http://www.duramag.com/, "Dura Magnetics, Inc.: Magnets and Magnet Solutions." World Wide Web, November 2003.

[11] F. Cardot, J. Gobet, M. Bogdanski, and F. Rudolf, "Fabrication of a magnetic transducter compsed of a high-density array of microelectromagnets with on-chip electronics," *Sensors and Actuators A*, vol. 43, pp. 11–16, 1994.

[12] Z. Griffith, K. Sundararajan, M. Dahlstrom, Y. Wei, N. Parthasarathy, and M. J. W. Rodwell, "80 Gb/sec TDM based fiber ICs designs using UCSB's InP DHBT technology," project report for MICRO project 00-083, Department of Electrical and Computer Engineering, University of California, University of California, Santa Barbara, California, 93106, 2001.

[13] W. A. Serdijn, A. C. van der Woerd, J. Davidse, and A. H. M. van Roermund, "A low-voltage low-power fully-integratable front-end for hearing instuments," *IEEE Transactions on Circuits and Systems I: Fundamental Theory and Applications*, vol. 42, pp. 920–932, November 1995.

[14] R. J. Baker, H. W. Li, and D. E. Boyce, *CMOS: Circuit Design, Layout, and Simulation.* John Wiley and Sons, Inc., 1998.

[15] B. Razavi, "Prospects of CMOS technology for high-speed optical communication circuits," *IEEE Journal of Solid-State Circuits*, vol. 37, pp. 1135–1145, September 2002.

[16] J. Hauptmann, F. Dielacher, R. Steiner, C. C. Enz, and F. Krummenacher, "A low-noise amplifier with automatic gain control and anticlipping control in CMOS technology," *IEEE Journal of Solid-State Circuits*, vol. 27, pp. 974–981, July 1992.

APPENDIX A

Directions for Setup of Agilent 35670A Spectral Analyzer

The experimental setup conditions for the Aglient 35670A are described below.

- **Frequency Setup**
  - Set Bandwidth to 12.8KHz
    1. FREQ Button
    2. STOP
    3. 12.8kHz
  - Set Resolution to 1600
    1. FREQ Button
    2. RESOLUTN(LINES)
    3. 1600
- **Function Setup**
  - Define Function
    1. ANALYS Button
    2. Define Function
    3. F1
    4. FFT(TIME1-TIME2)
  - Set Active Function
    1. MEAS DATA Button
    2. More Choices
    3. Math Function
    4. F1

- **Graph Setup**
  - Set Type of Data
    1. TRACE Coord Button
    2. Y Units
    3. Amplitude PK
  - Set Display of Data
    1. TRACE Coord Button
    2. LOG Magnitude
- **Get New Graph After GP-IB Capture**
  1. LOCAL/GP-IB Button
  2. Abort GP-IB
  3. START Button

APPENDIX B

Labview Subproject

Figure B.1 shows the front panel of the Labview environment. It includes a graph to make sure that the data received matches the data on the spectral analyzer. It also includes a prompt for the file to save the data. If no file is entered when the program runs, it will require the user to enter a filename at that time.

Figure B.2 shows the outer sequential programming structure. The first step in this sequential structure is the setup command for the GP-IB interactions. The GP-IB address of the spectral analyzer in this case is 16. The program sends the command `FORM ASC` over the GP-IB link to address 16. This command tells the spectral analyzer to send data in ASCII format.

Figure B.3 shows the second command of the outer sequential structure. This command contains an interior sequential structure. The first part of this interior sequential structure sends the command `CALC:X:DATA?` to the spectral analyzer (address 16). This command is a query command sent to the spectral analyzer asking for the data on the x axis.

Figure B.4 contains the second step of the interior sequential structure. The first step involves Labview reading a string of 32020 bytes off of the GP-IB bus. This is the number of bytes that the spectral analyzer will send assuming that the resolution has been set to 1600 as mentioned in Appendix A. That information will then be sent to two different places. The first part takes the string and replaces every instance of a ',' with a blank space. This allows easier importing into programs such as MatLab for data analysis. The edited string is then send to the file specified on the front panel.

The data also goes into a while looping structure. The purpose of this while structure is to extract all of the numbers from the string and put them into an array of numbers format. This array is then sent outside the interior sequential structure.

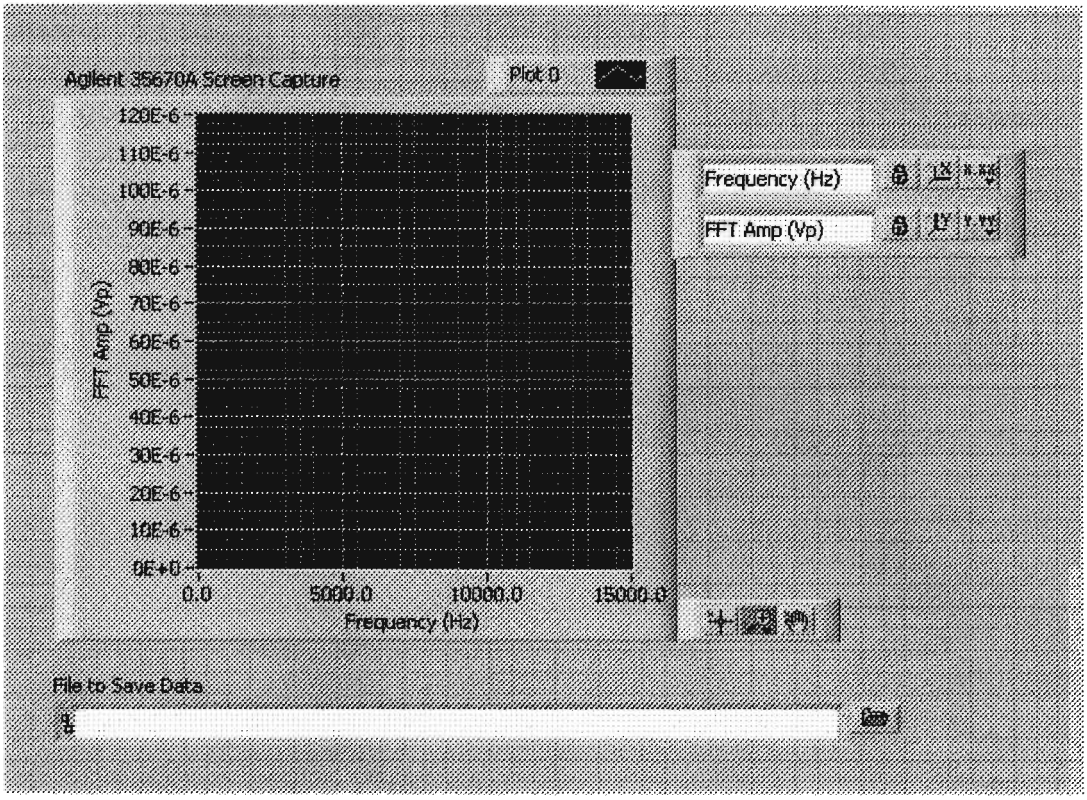

Figure B.1: Front Panel

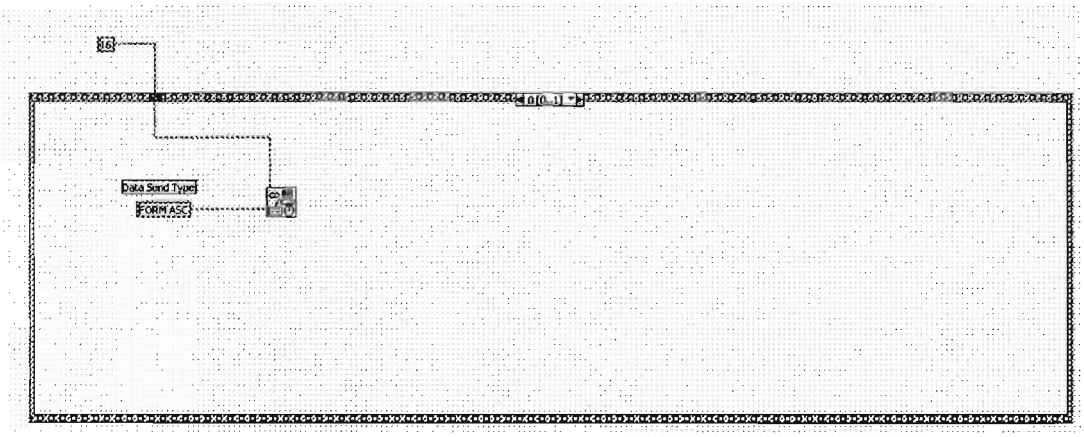

Figure B.2: GP-IB Setup

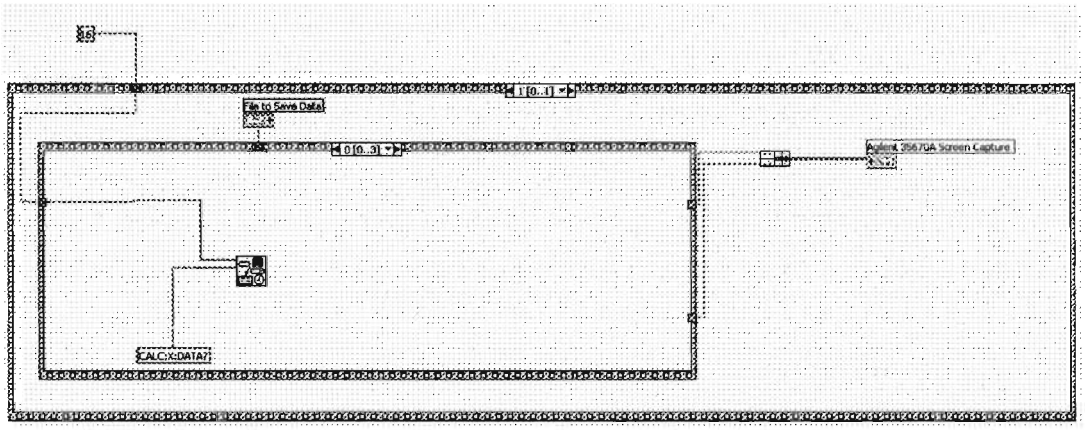

Figure B.3: Query X axis data.

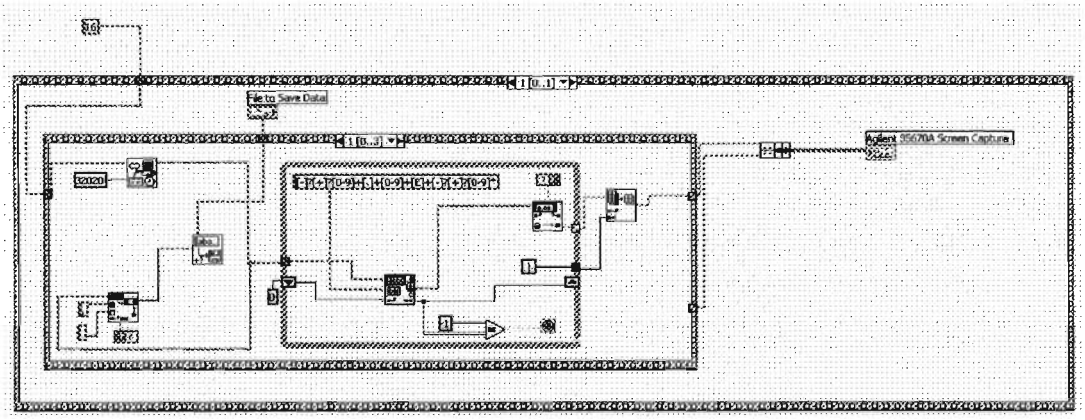

Figure B.4: Manipulate X axis data.

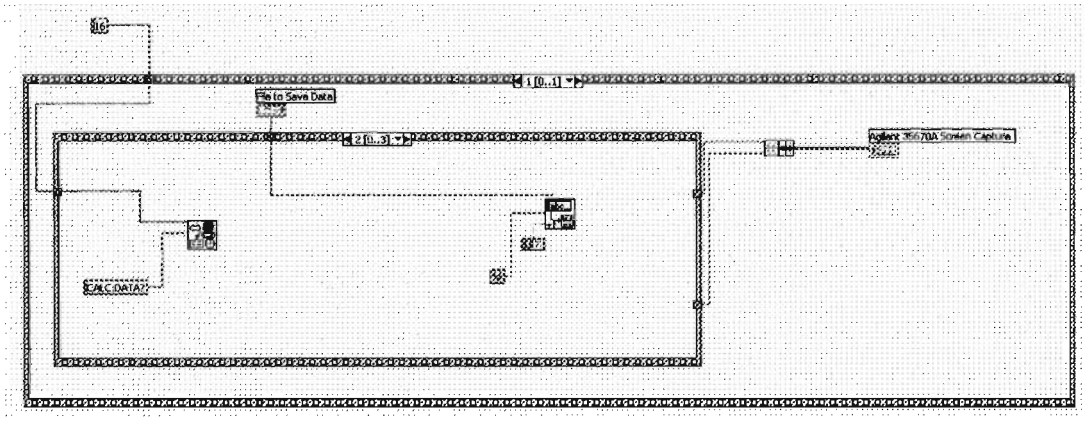

Figure B.5: Query Y axis data.

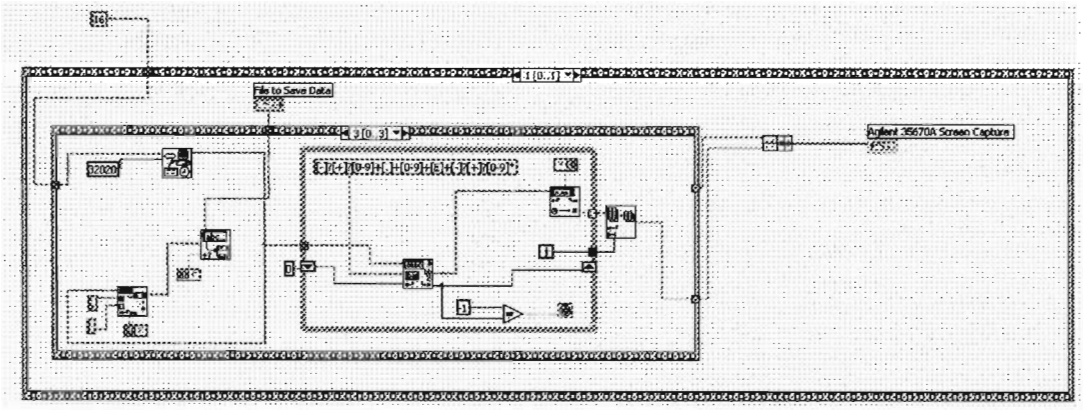

Figure B.6: Manipulate Y axis data.

Figure B.5 contains the third step of the interior sequential structure. This step sends the command CALC:DATA? to the spectral analyzer (address 16). This command is a query command sent to the spectral analyzer asking for the data on the y axis. This section also sends a CR/LF to the file containing the data. The 'T' needs to be added to this command so that the info is added together and not overwritten.

Figure B.6 contains the last step of the interior sequential structure. Labview read a string of 32020 bytes off of the GP-IB bus to get the y axis data. As before, the data string is modified by replacing every instance of a ',' with a blank space. This new string is then send to the end of the file specified on the front panel.

As before, all of the numbers from the string are extracted and put into an array of numbers format. This array is then sent outside the interior sequential structure where it is combined with the array of x axis values to form a bundle. This bundle is then sent to the graph on the front panel. At this point the data from the spectral analyzer is displayed on a graph on the machine running labview and the data is saved in a file specified on the front panel.

APPENDIX C

Pinouts & Bonding Diagrams

Name of Pin	I/O	Pin Number
4stage_out1	Output	28
4stage_out2	Output	29
3stage_out1	Output	32
3stage_out2	Output	31
ch_1s_out1	Output	17
ch_1s_out2	Output	16
ch_3s_out1	Output	25
ch_3s_out2	Output	24
ch_3sf_out1	Output	37
ch_3sf_out2	Output	38
ch_1s_in1	Input	18
ch_1s_in2	Input	19
ch_3s_in1	Input	22
ch_3s_in2	Input	23
ch_3sf_in1	Input	40
ch_3sf_in2	Input	39
f_out	Output	5
f_in	Input	6
gnd	I/O	4
gnd2	I/O	36
gnd3	I/O	30
vcc	I/O	20
vdd	I/O	3
vdda	I/O	21
vddd	I/O	1
vss	I/O	2

Table C.1: Cherry Hooper Pinout Table

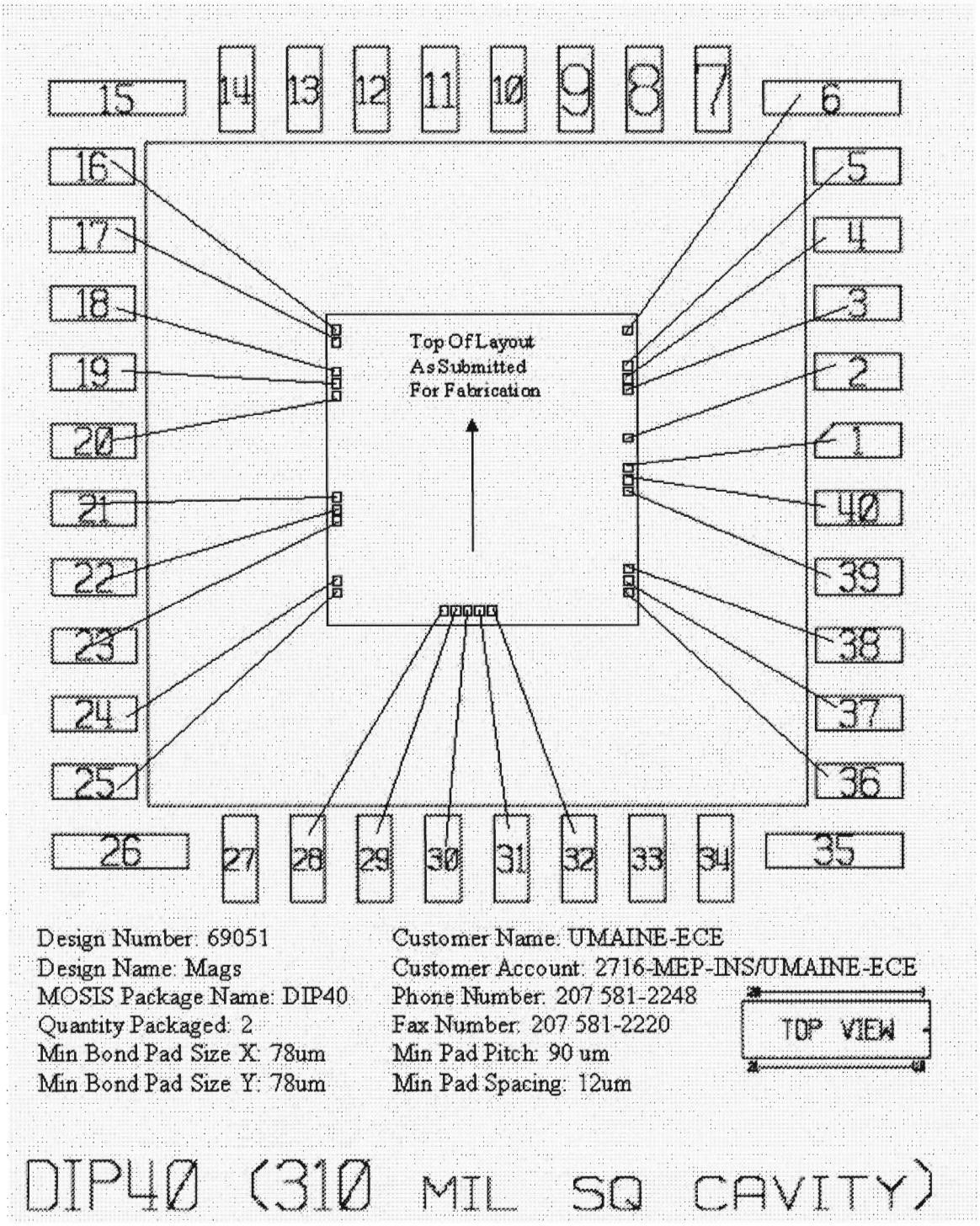

Figure C.1: Cherry Hooper Bonding Diagram

Name of Pin	I/O	Pin Number
tfull_pres_o	Output	24
tfull_pres_i	Input	23
tpre_o	Output	16
tpre_i	Input	15
tfull_o	Output	5
tfull_i	Input	6
res_io1	I/O	18
res_io2†	I/O	19
pre_o	Output	29
full_o	Output	31
gnd	I/O	30
gnda	I/O	25
gndd	I/O	4
vcc	I/O	3
vdd	I/O	40
vdda	I/O	26
vddd	I/O	17
vss	I/O	1

Table C.2: Single Ended Pinout Table
†Unnamed pin on layout

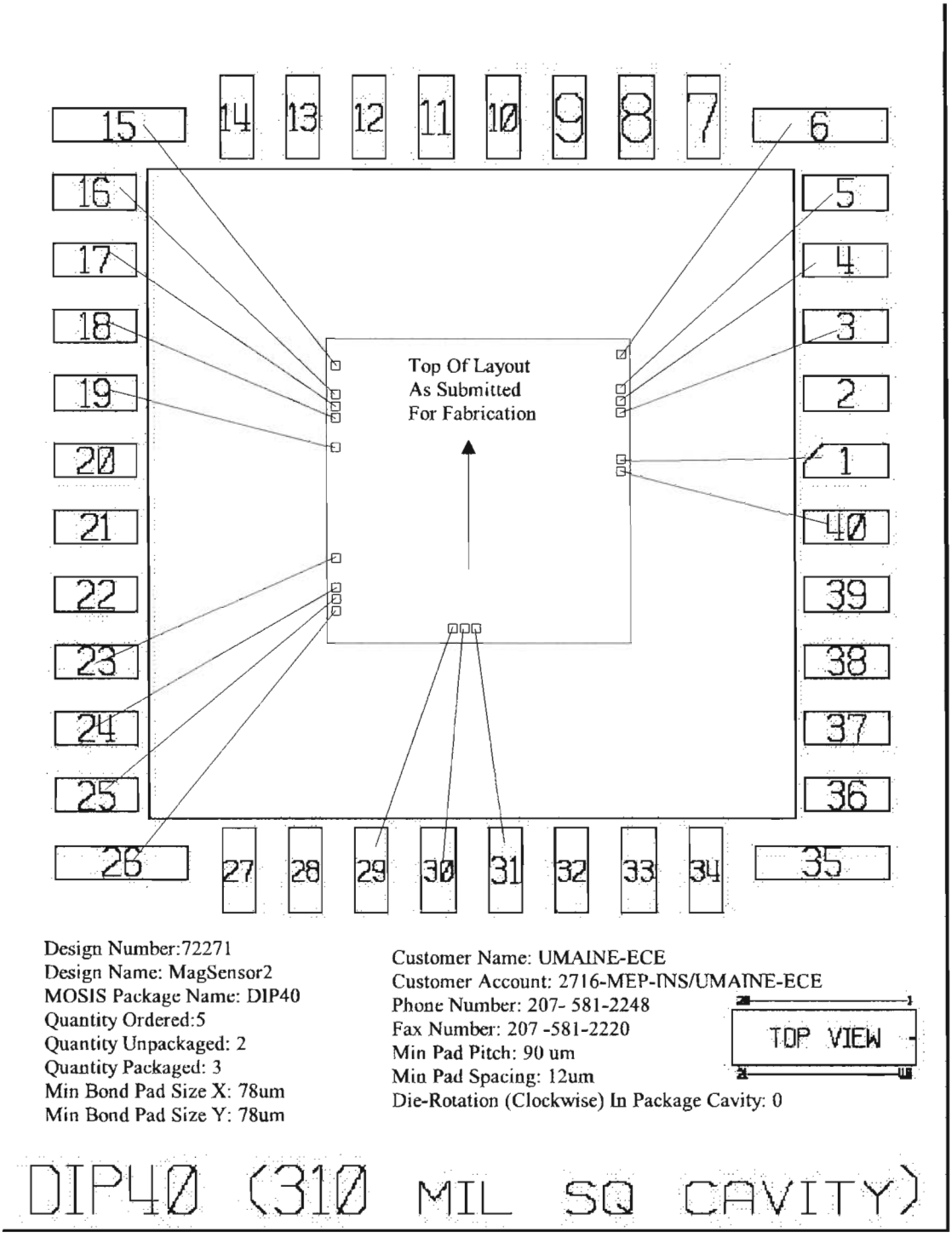

Figure C.2: Single Ended Bonding Diagram

BIOGRAPHY OF THE AUTHOR

Crystal R. Kenney was born in Waterville, Maine on July 16, 1981. She received her high school education from Erskine Academy in South China in 1999.

She entered the University of Maine in 1999 and obtained her Bachelor of Science degree in Computer Engineering and her Bachelor of Science degree in Engineering Physics in 2003.

In September 2003, she was enrolled for graduate study in Electrical Engineering at the University of Maine and served as a NSF GK-12 Fellow. Her current research interests include device physics and analog design. She is a member of IEEE, Tau Beta Pi, Eta Kappa Nu, Sigma Pi Sigma, and Golden Key, and her interests include fencing and jewelry design. At the conclusion of her Master's degree, she will pursue a Doctorate in Electrical Engineering at Stanford University. She is a candidate for the Master of Science degree in Electrical Engineering from The University of Maine in August, 2005.